SANDIA REPORT

SAND2005-4725
Unlimited Release
Printed August 2005

Total X-Ray Power Measurements in the Sandia LIGA Program

M. E. Malinowski, A. Ting

Prepared by
Sandia National Laboratories
Albuquerque, New Mexico 87185 and Livermore, California 94550

Sandia is a multiprogram laboratory operated by Sandia Corporation,
a Lockheed Martin Company, for the United States Department of Energy's
National Nuclear Security Administration under Contract DE-AC04-94AL85000.

Sandia National Laboratories

Issued by Sandia National Laboratories, operated for the United States Department of Energy by Sandia Corporation.

Available to DOE and DOE contractors from
U.S. Department of Energy
Office of Scientific and Technical Information
P.O. Box 62
Oak Ridge, TN 37831

Telephone: (865)576-8401
Facsimile: (865)576-5728
E-Mail: reports@adonis.osti.gov
Online ordering: http://www.osti.gov/bridge

Available to the public from
U.S. Department of Commerce
National Technical Information Service
5285 Port Royal Rd
Springfield, VA 22161

Telephone: (800)553-6847
Facsimile: (703)605-6900
E-Mail: orders@ntis.fedworld.gov
Online order: http://www.ntis.gov/help/ordermethods.asp?loc=7-4-0#online

SAND2005-4725
Unlimited Release
Printed August 2005

Total X-ray Power Measurements in the Sandia LIGA Program

M. E. Malinowski
Microsystems Processing Department 8753

A. Ting
Engineering Sciences and Technologies Department 8775
Sandia National Laboratories
P.O. Box 969
Livermore, CA 94551-0969

ABSTRACT

Total X-ray power measurements using aluminum block calorimetry and other techniques were made at LIGA X-ray scanner synchrotron beamlines located at both the Advanced Light Source (ALS) and the Advanced Photon Source (APS). This block calorimetry work was initially performed on the LIGA beamline 3.3.1 of the ALS to provide experimental checks of predictions of the LEX-D (**L**IGA **EX**posure-**D**evelopment) code for LIGA X-ray exposures, version 7.56, the version of the code in use at the time calorimetry was done. These experiments showed that it was necessary to use bend magnet field strengths and electron storage ring energies different from the default values originally in the code in order to obtain good agreement between experiment and theory. The results indicated that agreement between LEX-D predictions and experiment could be as good as 5% only if (1) more accurate values of the ring energies, (2) local values of the magnet field at the beamline source point, and (3) the NIST database for X-ray / materials interactions were used as code inputs. These local magnetic field value and accurate ring energies, together with NIST database, are now defaults in the newest release of LEX-D, version 7.61. Three dimensional simulations of the temperature distributions in the aluminum calorimeter block for a typical ALS power measurement were made with the ABAQUS code and found to be in good agreement with the experimental temperature data. As an

application of the block calorimetry technique, the X-ray power exiting the mirror in place at a LIGA scanner located at the APS beamline 10 BM was measured with a calorimeter similar to the one used at the ALS. The overall results at the APS demonstrated the utility of calorimetry in helping to characterize the total X-ray power in LIGA beamlines. In addition to the block calorimetry work at the ALS and APS, a preliminary comparison of the use of heat flux sensors, photodiodes and modified beam calorimeters as total X-ray power monitors was made at the ALS, beamline 3.3.1. This work showed that a modification of a commercially available, heat flux sensor could result in a simple, direct reading beam power meter that could be a useful for monitoring total X-ray power in Sandia's LIGA exposure stations at the ALS, APS and Stanford Synchrotron Radiation Laboratory (SSRL).

Acknowledgment

This work was performed as part of the LIGA program at Sandia National Laboratories, Livermore, CA. Sandia is a multiprogram laboratory operated by Sandia Corporation, a Lockheed Martin Company, for the United States Department of Energy under Contract DE-AC04-94AL85000. All experimental work was performed at The Advanced Light Source, Lawrence Berkeley National Laboratory, Berkeley, CA. The Advanced Light Source is supported by the Director, Office of Science, Office of Basic Energy Sciences, Materials Sciences Division, of the U.S. Department of Energy under Contract No. DE-AC03-76SF00098 at Lawrence Berkeley National Laboratory. The ring parameter inputs provided by Christoph Steier of the ALS Accelerator Physics Group were essential to this work and Christoph's ready collaboration was greatly appreciated. Cheryl Hauck of the ALS helped with some of the experiments and with the care and feeding of the vacuum and air scanner systems. Stewart Griffiths provided a pre-release upgrade to LEX-D 7.56. Discussions with Georg Aigeldinger regarding his past calorimetry work and Georg's and Stewart's critical readings of this manuscript are appreciated. Dawn Skala supplied some of the PMMA samples used in this work.

This page intentionally left blank.

Table of Contents

This page intentionally left blank.

List of Figures

List of Tables

This page intentionally left blank.

Nomenclature

ALS	Advanced Light Source (synchrotron)
APS	Advanced Photon Source (synchrotron)
BL	beamline
B (*T*)	magnetic field (Tesla)
C	heat capacity (J/K)
^{o}C	degrees Centigrade
GeV	Giga electron volts (10^{9} volts)
HFS	Heat flux sensor
Hz	Hertz (cycles/s)
P	power (Watt)
PMMA	poly (methyl methacrylate)
PD	photodiode
SSRL	Stanford Synchrotron Radiation Laboratory
T	temperature
t	time
TC	thermocouple

This page intentionally left blank.

1. Introduction

1.1 Background

At the Advanced Light Source (ALS) synchrotron, Lawrence Berkeley National Laboratory, a linear stage, vacuum scanner has been constructed for the exposure of samples in the LIGA program of Sandia National Laboratories. This vacuum scanner has been constructed on beamline (BL) 3.3.1, adjacent to an existing LIGA exposure station located on beamline 3.3.2 and operating under atmospheric conditions. Both beamlines receive X-rays from the common front end located in the "Sector 3" bend magnet of the ALS. As part of the characterization of the exposure system, calorimetry measurements were performed to determine the total X-ray power delivered to the vacuum scanner. These measurements were then compared to the predictions of the computer code LEX-D 7.56, the code used to determine dose values in the SNL LIGA prototyping program at the time the calorimetry measurements were taken (Summer, 2004). These initial studies of the X-ray power of beamline 3.3.1 advanced into a more detailed investigation of practical, X-ray power measurements relevant to Sandia's LIGA program. This report documents this work, and is divided into three topics: The first (Sections 2,3) describes these measurements on beamline 3.3.1 and the ABAQUS thermal modeling results for the beam-plate calorimeter used; the second topic (Section 4) gives details on how similar calorimetry methods were used to help characterize the total X-ray power at another LIGA beamline, 10 BM at the Advanced Photon Source (APS); and the third topic (Section 5) relates how these calorimetry experiments provided the impetus for exploring methods other than simple calorimetry for measuring total X-ray powers in bend magnet beamlines. This section describes both the different methods tested and the results from the initial power measurement with the novel methods.

In the LIGA prototyping program, when a PMMA photoresist sample is exposed, different sample, scanner and synchrotron input parameters are entered into LEX-D to determine the correct dose value for proper exposure of the PMMA: examples of such parameters include bottom dose, the scan speed, scan length, PMMA thickness, and X-ray filters used in the exposure. However, in addition to these parameters particular to the scan being performed, certain ALS synchrotron parameters are used as default inputs for the LEX-D calculation. These ring parameters are rarely changed in day to day dose computations using LEX-D. The two fundamental synchrotron parameters which define the X-ray spectrum of a bend magnet beam are the magnetic field (or radius) and the energy of the electrons in the storage ring.

In a 10° bend magnet at the ALS, the magnet type which serves the ALS LIGA beamlines, the electron trajectories are not simple, circular arcs, but are more complicated because the bend magnetic field varies radially (measured with respect to the center of the ALS ring) and the resulting electron orbit has a different, effective radius at different angular (and radial) positions in the bend magnet. Since the radiation delivered to the 3.3.1 LIGA beamlines originates from one source, or tangency point, in the electron beam orbit within the magnet, it is important to use this local radius (or magnetic field) as the input for LEX-D calculations. Also important to the correct dose

predictions using LEX-D is inputting the correct beam energy. Section 2 below in this report describes the results of performing experimental, total power calorimetry measurements on BL 3.3.1 and comparing these results to the predicted total powers using LEX-D 7.56 with two different sets of input ring parameters: the first set, called the "old" set in discussions below, is comprised of the default parameters for the ALS used in LEX-D 7.56; the second set, called the "new" set, consists of values which represent the values recommended by the ALS Accelerator Group[1] for both the electron energy and local magnetic field in the bend magnet serving the SNL LIGA beamlines.

1.2 Radiated power and ALS ring parameters

To help provide a simplified picture of how values of the ring energy and magnetic field in the ALS beamline 3 bend magnet influence power and, hence, exposure conditions with no inline X-ray filtering, it is helpful to examine the electron energy and field dependence of the total power radiated by a circular electron ring: The total power, P (kW), radiated by an electron ring current I (A) with electron energy E (GeV) in a constant magnet field, B (*T*) is given by the following equation[2]:

(1) $P = 26.6 \cdot E^3 \cdot B \cdot I$

Thus, the power radiated from a bend magnet is most influenced by changes in electron energy, followed by changes in the magnetic field and ring current, which are linear. In the ALS, the ring current decays, typically from a maximum of about 400 mA to about 200 mA, at which point additional electrons are injected, or "filled," into the ring. At 1.9 GeV nominal ring energy, the most commonly used electron energy at the ALS, the time between fills is approximately 8 hours. At 1.5 GeV, the second, least used ring energy, the time between fills is about 5 hours.

Based on equation (1) above, for the same ring current, the ratio, **R**, of total powers radiated from a bend magnet operating at different electron energies and magnetic fields would be given by the following:

(2) $\mathbf{R} = (P_{old} / P_{new}) = (E_{old} / E_{new})^3 \cdot (B_{old} / B_{new})$

It is instructive to compare the "old" versus "new" values for the ring energy (E) and the magnetic field (B); the "old" values were the default values used in LEX-D v7.56, the version in use at the time the first calorimetry experiments were started. Table 1 below gives both sets of these values in the third and forth columns. The "new" values for both the local magnetic field at the BL3.3.1 tangency point and the average ring energy are values recommended by the ALS accelerator Group[1].

The last column in the table lists these total, unfiltered radiated power ratios. These ratios predicted by equation (2) would be about 6% higher (1.9 GeV) and 1% lower (1.5 GeV) when using "old" versus "new" ring input values. The corresponding LEX-D predictions are for these same power ratios are basically the same as given from equation (2).

TABLE 1. "Old" versus "New" ALS parameters.

VALUES	NOMINAL ENERGY	"OLD" VALUES (LEX-D 7.56 DEFAULTS)	"NEW" VALUES	POWER RATIO* "OLD"/"NEW'
E [GeV]	1.9	1.90	1.894 +/- 0.001	1.062
B [T]		1.32	1.255	
E [GeV]	1.5	1.50	1.522 +/- 0.001	0.988
B [T]		1.04	1.007	
* Unfiltered from synchrotron				

At 1.9 nominal GeV operation both the "new" ring energy and magnetic fields are lower than the corresponding "old" values. At 1.5 GeV nominal energy, the "new" ring energy is higher, the new magnetic field, lower, than the respective "old" values. The photon energy spectra predicted by LEX-D 7.56 for unfiltered and selected filtered cases are shown in the uppermost curves in Figure 1 for the ALS running at a nominal 1.9 GeV. Since most of the exposures on the LIGA scanner are performed at 1.9 GeV nominal energy, the values in the table and equation (1) predict lower overall radiated powers using "new" (red) values compared to "old" (blue) values. In addition, since the effective magnetic field is lower in the "new" value set, the predicted spectrum will be expected to contain fewer higher energy photons using "new" values. Figure 1 shows the effects of increased filtering on the power spectra predicted using these "old" and "new" data sets. The minimum amount of filtering possible in BL 3.3.1 is 254 μm of Be, which is the sum of the thicknesses of a water-cooled, Be filter in the ultrahigh (UHV) vacuum beamline upstream and the Be window which forms the vacuum break between the vacuum scanner chamber and the UHV beamline. Each window is 127 μm thick. As the figure shows, adding even more filters than 254 μm of Be – 147.6 μm of aluminum- further increases the average photon energies ("hardens") the spectra and makes the differences between the predicted spectra using the "new" vs. "old" values even greater.

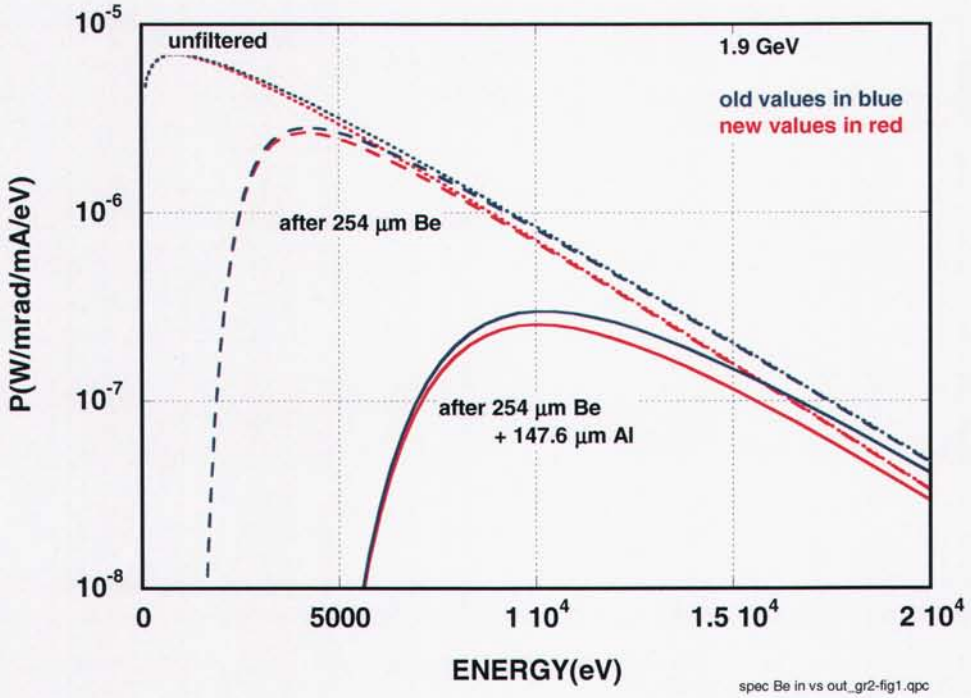

Figure 1. **Power Spectrum for ALS (1.9 GeV nominal), different filtering predicted by LEX-D using "new" and "old" ALS E and B Values.**

Thus, these simple results underscore the importance of experimentally benchmarking the LEX-D code. When LEX-D 7.56 is used in discussions below, there are basically 4 variants which are used: The different versions depend not only on the ring parameter input ("old"-default- vs. "new") used, but also on the X-ray attenuation database – "Biggs" (default)[3, 4] or "NIST"[5] –that is used.

2. Calorimetry Studies in the LIGA Vacuum Scanner, Beamline 3.3.1, Advanced Light Source

2.1 Experimental Arrangement

The basis of the total power measurement is block calorimetry[6], in which the rate of rise in temperature of a nearly thermally isolated aluminum block is measured when the X-ray beam hits the block. A simplified schematic of the experimental arrangement is shown in Figure 2 below. When LIGA prototyping samples are exposed in the vacuum scanner, there is a low pressure of helium gas, typically about 100 Torr, a condition chosen both to help minimize undesirable oxidation of LIGA exposure station components and to promote thermal cooling of LIGA PMMA substrate and the X-ray mask. However, in the current work all aluminum block calorimetry work was performed under "vacuum" (pressures no higher than 0.050 Torr) to minimize thermal conduction losses from the calorimeter beam plate.

The X-ray beam from the beamline beam magnet passes through two beryllium windows (127 μm thick each) and a filter (varies depending on the experiment) and hits the aluminum block, or "beam plate." This aluminum block is supported by 2 Nylon standoffs to an aluminum base plate. This base plate is in turn attached to an actively water-cooled, copper mounting platform which is on the linear stage in the vacuum chamber of the vacuum scanner. Although this cooling is not essential to the calorimetry work, it is used to cool substrates during LIGA exposures; in the calorimetry modeling it results in the thermal boundary condition of 21.5 ^{o}C at the baseplate when ABAQUS modeling (Section 3) was performed. Thermocouples monitor both the beam plate and base plate temperatures before, during, and after the X-ray beam is allowed to hit the beam plate by the opening/closing of a shutter upstream in the ultrahigh vacuum (UHV) beamline connecting the vacuum scanner chamber to the ALS ring. The beam plate thermocouple (type "K") is mounted with thermally conductive epoxy into a small hole, located in the center of the back of the beam plate; the hole has a depth of about one third of the beam plate thickness.

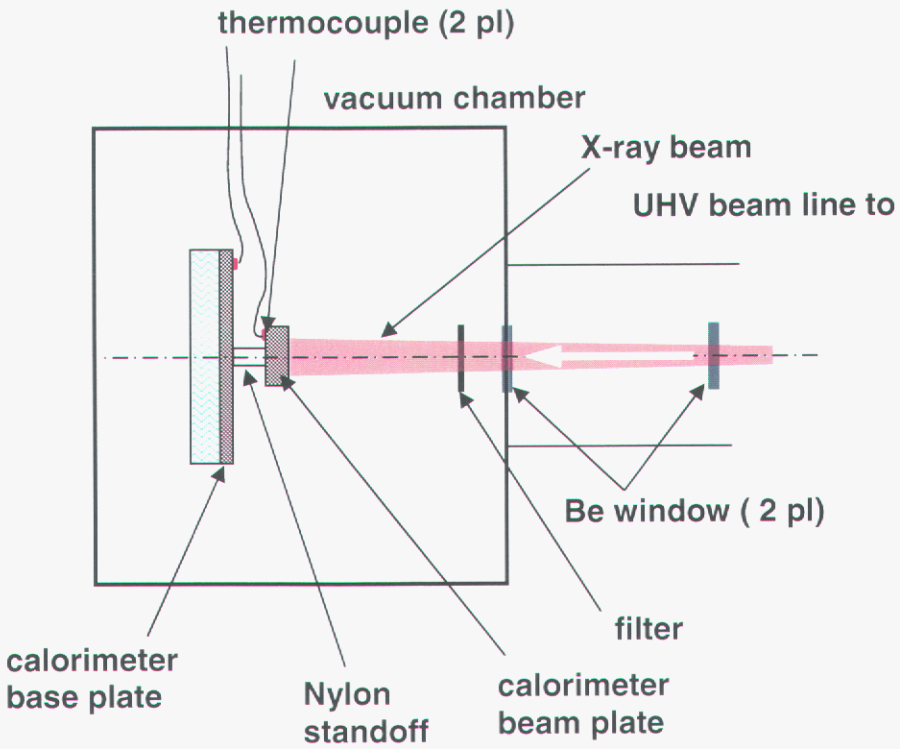

Figure 2. Simplified Schematic of Experimental Setup (Side view)

A photograph of the calorimeter assembly in place on the linear stage platform is shown in Figure 3 below. The "wire shield" is a thick, copper foil put over the insulated thermocouple leads in order to shield the leads from the X-ray beam.

Based on beamline specifications, each Be window in the UHV beamline is estimated to be 127 μm thick. Thus, even when no filters are introduced in the beam path inside of the vacuum chamber, the X-rays travel through 254μm of Be. When results with filters are described below, these filters are in addition to the two Be windows that are always present. Beamplates in all calorimeters were made of aluminum in order to minimize reradiated power through fluorescence radiation, estimated by LEX-D calculations to be less than about 0.2% of the incident power. Using copper as a beam plate material can result in up to ~5% of the incident power being reradiated as copper K_α radiation, an undesirable situation since the reradiated power complicates accurate computation of the power balance in the tests.

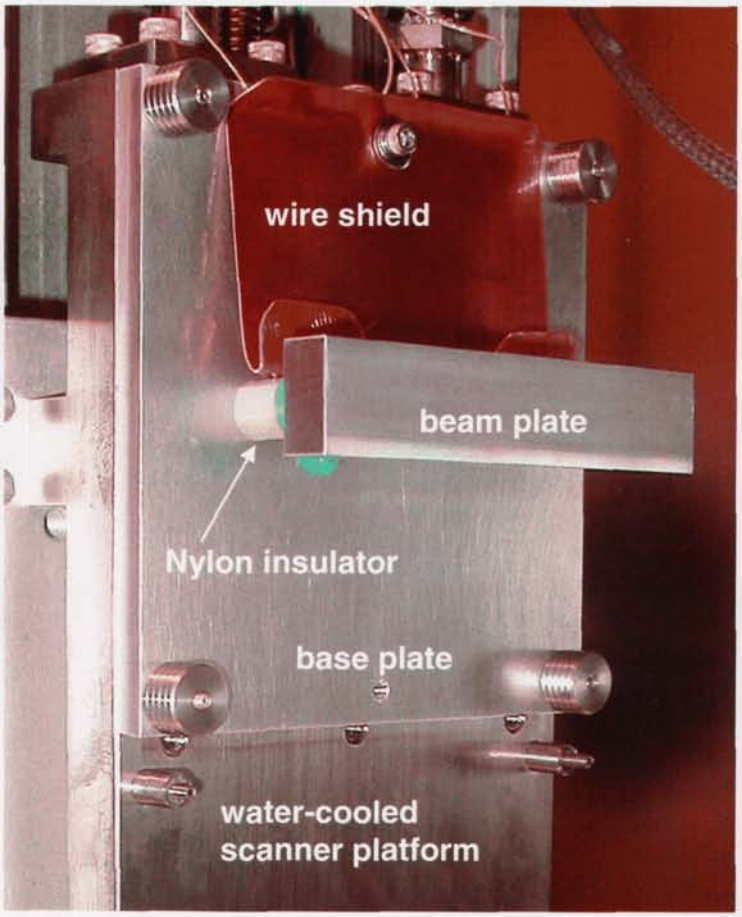

Figure 3. Photograph of Calorimeter in place on scanner.

Although several different aluminum beam plates were used in different experiments, every beam plate was at least 10 mm thick. LEX-D calculations indicated that this aluminum thickness would absorb at least 99.9% of the incident power for any of the filter sets used in the current experiments. The X-ray beam was intentionally truncated horizontally by a 4 mm thick copper aperture in order to help minimize the influence of rounded end effects on power calculations. The untruncated beam has a width about 100 mm, while the truncated beam has a measured width of 90 mm. Vertically the beam was not truncated. A photograph of a beam pattern taken by X-ray sensitive film is shown in Figure 4 below.

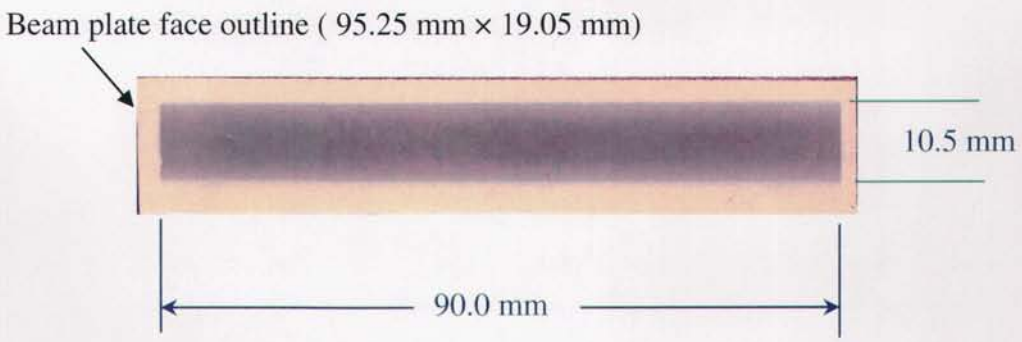

Figure 4. **X-ray beam pattern taken by X-ray sensitive film which was mounted onto the face of calorimeter beam plate**

The beam plate outline is indicated in the figure, and the beam pattern produced by the X-ray beam is the dark, blue rectangle. As the figure shows, the horizontal extent of the beam pattern is sharply truncated; the vertical extent of the beam is about 10.5 mm, corresponding to an effective, vertical angular beam divergence (out of synchrotron plane) of about $\pm$ 0.30 milliradians.

2.2 Experimental data acquisition and analysis

Aluminum block calorimetry is based on determining a rate of temperature rise in the aluminum beam plate before, during and after the time that the X-rays hit the beam plate. Figure 5 shows the temperatures during one typical calorimetry sequence. Temperature readings were logged to a computer at 2 second intervals. The temperature readings from the two thermocouples were calibrated with a high precision, high accuracy, low voltage source designed for simulating thermocouple inputs[7]. Both experimental results and thermal modeling (Section 3) demonstrated that the combined thermocouple-calorimeter response time was short enough to accurately measure power inputs.

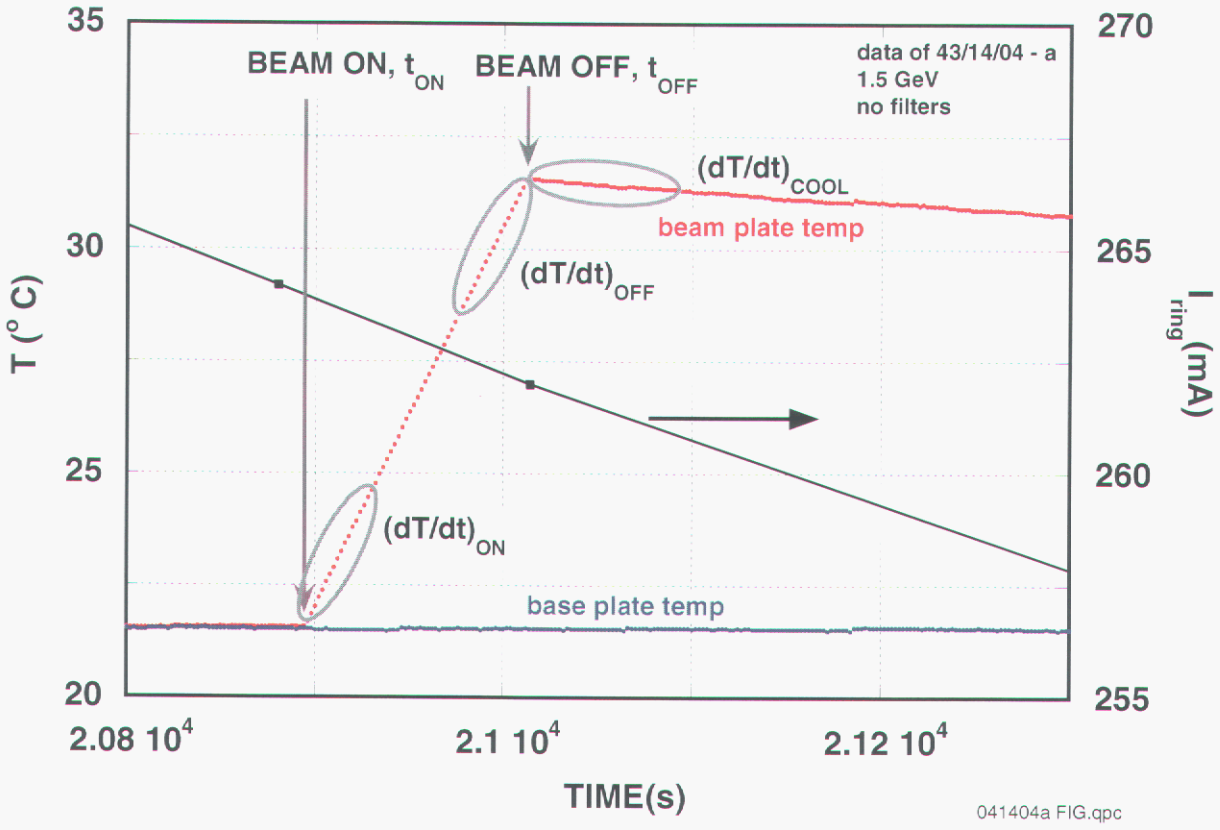

Figure 5. **Temperature-time behavior of beam and base plate during one calorimetry run.**

Initially the temperatures of both the base and beam plates are essentially constant and nearly equal to each other. During the time the X-rays hit the beam plate, there is an approximately linear increase in temperature with time; when the beam is turned off, there is a slow cooling of the beam plate. Detailed examination of the temperature-time characteristic reveals deviations from linearity due to the effects of (1) radiation (the dominant power loss in vacuum) and (2) decreases in the input X-ray power caused by decay of the synchrotron ring current. Note that during these experiments, the temperature of the base plate was essentially unchanged during X-ray exposure of the beam plate because of the thermal isolation provided by the nylon standoffs holding the beam plate to the baseplate and the water cooling

In Figure 5 the ring current is also shown, and it is clearly decreasing (about 3% in the example shown) during the time the beam plate is being heated. The amount of decrease in the ring current during the heating time depends not only on the total time the plate is heated but also on the time during the synchrotron ring cycle that the calorimetry is performed, since the rate of ring current drop is largest immediately after a fill of the electron storage ring.In the current work, the power inputs were determined at both the times the heating started ("beam on") and stopped ("beam off"). The starting point for these calculations is the determinations of the effective slopes of the

temperature-time responses at these two points. These slopes were determined by making a linear fit to the temperature characteristic and computing the slope from the fit. Examples of these slopes are given in Figure 5 and defined as follows:

$(dT/dt)_{ON} \equiv$
slope from linear fit to T vs. time over the interval $\{t_{ON} \rightarrow t_{ON} + 0.25(t_{OFF} - t_{ON})\}$;
$(dT/dt)_{OFF} \equiv$
slope from linear fit to T vs. time over the interval $\{ t_{OFF} - 0.25(t_{OFF} - t_{ON}) \rightarrow t_{OFF} \}$;
and
$(dT/dt)_{COOL} \equiv$
slope from linear fit to T vs. time over the interval $\{ t_{OFF} \rightarrow t_{OFF} + 100s.25(t_{OFF} - t_{ON}) \}$.

A minimum of 8 data points were used to make these slope calculations. Since data were acquired at a 2 second sampling rate, in the case of rapid temperature increases, this required that the starting and ending slope sampling regions were sometimes greater than 25% of the total temperature rise region. The power inputs were calculated at the start and end of each heating cycle and normalized to 320 mA ring current as follows:

(3a) $P(t_{ON}) = M \cdot c \cdot (320/I\,(t_{ON})) \cdot (dT/dt)_{ON}$;
(3b) $P(t_{OFF}) = M \cdot c \cdot (320/I\,(t_{OFF})) \cdot [(dT/dt)_{OFF} - (dT/dt)_{COOL}]$
$= M \cdot c \cdot (320/I\,(t_{OFF})) \cdot (dT/dt)_{Off\text{-}effective}$

where c = the specific heat of aluminum = 0.90 J/g-K,
M = the aluminum beam plate mass (could vary from run to run);
I(t) = the ring current at the "ON" or "OFF" times;
$(dT/dt)_{Off\text{-}effective} = [(dT/dt)_{OFF} - (dT/dt)_{COOL}]$.

The powers calculated by (3a) and (3b) typically differed by no more that about 3%. In practice, it is simplest to determine powers from the temperature versus time characteristic just after heating (starts-equation (3a))since both radiative and conductive losses are negligible during this time. Note that (3b) above explicitly accounts for heat loss due to cooling of the block at the time t_{OFF}; the magnitude of this cooling rate is typically no more that about 10% of the heating rate at the same time. A short discussion of cooling is given in Appendix A.

It is instructive to estimate the errors in calculating power by the above equations. The sources of error in equation (3a) are estimated as follows:

- M, mass of Al block - The aluminum beam plate masses were not all the same, but were measured before each run when the plate was changed. These masses ranged from about 49.71 g to 132.14 g, and could be measured to uncertainties better than about 0.1 g, an error of at most about 0.2%.
- c, specific heat of aluminum. The maximum uncertainty in the assumed heat capacity is estimated to be 1%.
- I (t_{on}), ring current – known to better than about 0.2 ma, or <0.1% of the total ring current.
- (dT/dt), the computed slope- estimated to be a maximum of about 2 %, based on the results of the linear fits to the slopes.

All of these errors should be independent, and the estimated total percentage error should be approximately $((0.2)^2 + 1^2 + (0.1)^2 + 2^2)^{1/2}$, or about 2.3%. In the experimental results described below this number rounded up to 3%.

2.3 Experiments - filters Used

Six separate experimental runs with four different beam calorimeter plates were conducted. A total of 26 separate calorimetry experiments, each with results similar to those shown in Figure 5, were performed with a variety of filters. The filter combinations used in each calorimetry run, together with the number of measurements taken with that filter combination, are listed in Table 2 below (all filters are in addition to the 254 μm of Be). Note that each filter combination is also assigned an identification number ("I.D. No."). This I.D. number increases with increasing filtering and is used to help identify the data results.

The majority of the work was performed at nominal ring energies of 1.9 GeV. When filters were used, they consisted of aluminum foil, or combinations of aluminum foil and PMMA or Kapton. A variety of thicknesses of filters were used; all thicknesses were determined by cutting a large area of the foil, weighing the foil, and determining the thickness using material density. The densities assumed for the different filter materials are as follows:

Aluminum	2.70 g/cm^3
PMMA	1.19 g/cm^3
Kapton	1.42 g/cm^3

A total of 25 separate calorimetry experiments were performed in six different experimental runs at the beamline over the period of 3 months. Four different beam plates and thermocouple combinations were used; some filter combinations (I. D. numbers1,2,3,5,6 in Table 2) were repeated at different times.

TABLE 2. Filters used in the Calorimetry experiments

I.D. No.	FILTERS USED*	No. OF EXPERIMENTS, NOTES
1	NONE	7, 1 exp. at 1.5 GeV
2	5.8 μm Al	2, 1 exp. at 1.5 GeV
3	38.8 μm Al	2, 1 exp. at 1.5 GeV
4	49.2 μm Al	1
5	98.4 μm Al	3
6	147.6 μm Al	4
7	147.6 μm Al + 500 μm PMMA	1
8	147.6 μm Al + 512 μm KAPTON	1
9	147.6 μm Al + 1000 μm PMMA	1
10	147.6 μm Al + 1500 μm PMMA	1
11	147.6 μm Al + 1524 μm PMMA	1
12	147.6 μm Al + 3024 μm PMMA	1

*In addition to 254 μm of Be

2.4 Results

The experimental results were compared to the predictions of total power given by LEX-D 7.56. LEX-D was used to predict the total power into the calorimeter beam block using the "old," or default beam parameters and the "new" beam parameters. In addition, for "new" beam parameters, predictions using both the Biggs and NIST attenuation databases were obtained. Step-by-step procedures for performing the calculations are given in Appendix B.

With each different filter set and ring energy listed in Table 3, LEX-D predictions using "old" and "new" values from Table 1 were made. The ratio of the (experimentally measured power) / (LEX-D predicted power) was computed for every experimental calorimeter run.

After the calculations were performed for each calorimetry run, the experimentally determined X-ray power was divided by the power predicted by LEX-D. The resulting ratios are plotted in Figure 6 for both 1.5 GeV ring operation experiments and for the more common 1.9 GeV experiments; the data points are shown plotted with +/- 3% error

bars. All the numerical values for both experiment and theory are also listed in a table in Appendix C. Both in Figure 6 and in the Appendix the following, different (experiment/theory) values using LEX-D predictions were made:

- "old" ring values, Biggs database (default LEX-D 7.56 configuration- solid, blue circles in Figure 6);
- "new" ring values, Biggs database (open, red squares); and
- "new" ring values, NIST database (solid, red squares).

The upper panel in the figure shows the results for 1.9 GeV ring energy, the energy most used during SNL LIGA exposures; the lower panel shows the results for 1.5 GeV operation. The power ratio points are plotted versus the "I.D. Number" of each filter combination. Note that the filters used are explicitly indicated above the I.D. Number in the upper plot panel.

The 1.5 GeV results show that there is essentially no difference in total powers predicted using the "old" or "new" bend magnets using the same Biggs database; in addition, there is good agreement between experiment and predictions, with the ratio of ($P_{expermental}$ / P_{LEX-D}) ranging from about 0.95 to 0.98. There seems to be a slight decrease in agreement going from "no filters" to 38.8 μm Al filter (index 1→ 2→3), but more data are required to establish this trend.

Note that this agreement between the results of predictions using the two data sets might be expected from the ratio predicted for the unfiltered (No Be windows) powers at 1.5 GeV, which predicted (see rightmost column, Table 1) (P_{OLD} / P_{NEW}) =0.988. The 1.9 GeV results show that the "new" values give substantially better agreement between theory and experimental power values than when using the "old" values: When these "new" bend magnet and ring energy values and the Biggs database are used, the ratio ($P_{expermental}$ / P_{LEX-D}) ranges from about 0.94 to 1.05 except for the thickest filter set. When the "old" values are used, however, the ratio of ($P_{expermental}$ / P_{LEX-D}) decreases from about 0.9 (no filtering – I.D. #1) to about 0.77 when 147.6 μm of Al filtering is used. Increased filtering – in the form of PMMA or Kapton – had no further effect on this ratio. These data, taken together with the results suggest a decrease in predicted power accuracy with increasing Al thickness when using the Biggs database. Note that there is no such trend when using the NIST database, suggesting that the Biggs database values for aluminum may not be as accurate as the corresponding NIST values.

The differences between the ($P_{expermental}$ / P_{LEX-D}) data at 1.9 GeV are significantly larger than any experimental errors, which are estimated to be about $\pm$3 % and are shown by the error bars in the Figure. The trend in increasing ($P_{expermental}$ / P_{LEX-D}) for the thickest three filters is not understood at this time. However, both the sample uniformities and the thicknesses of these thickest PMMA + Al combinations were not

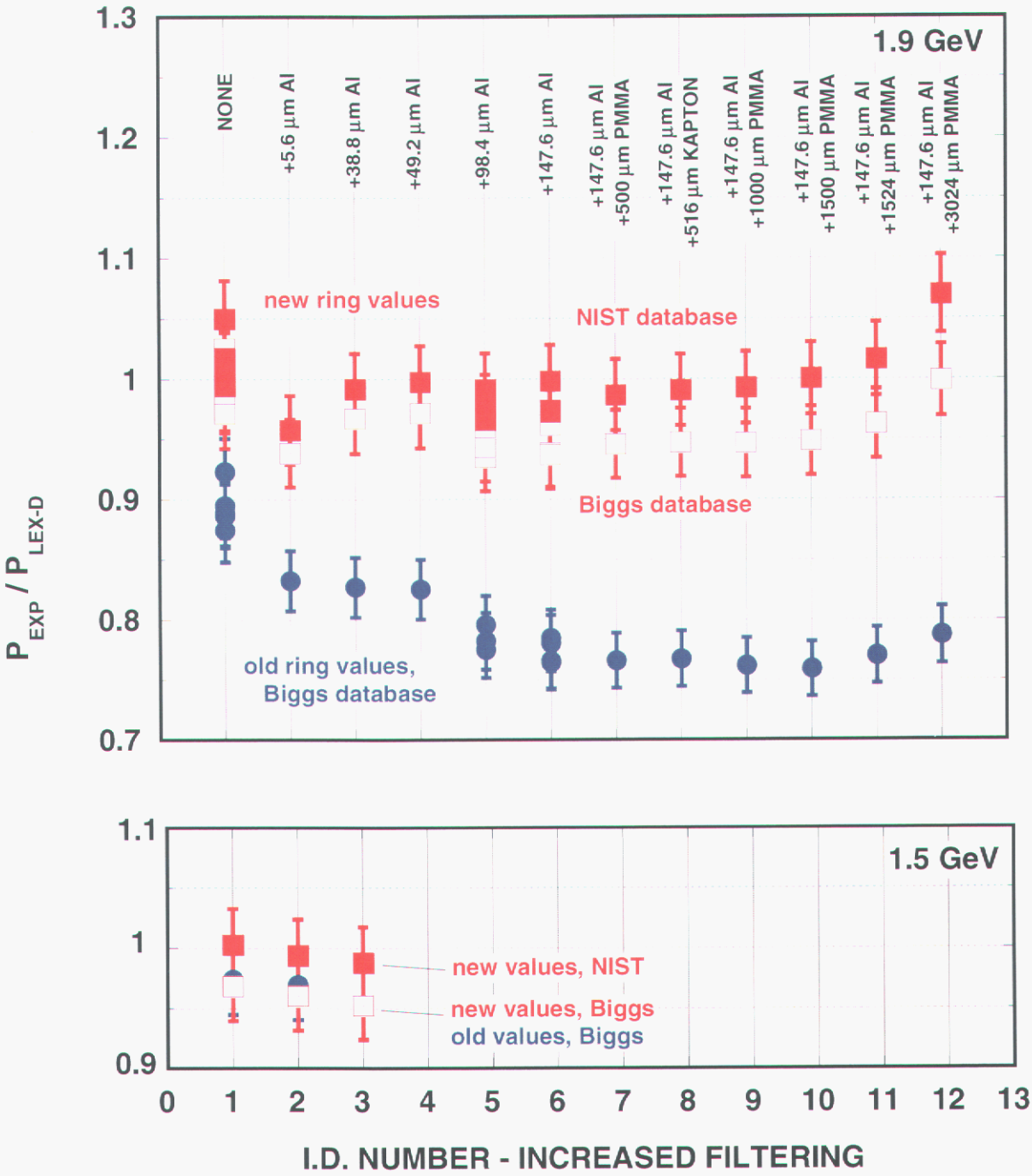

Figure 6. Ratio of (experimentally measured power)/ (LEX-D predicted powers) for all experiments listed in Table 2. The filter combinations (in addition to 254 µm Be) are given above the respective data points. The upper panel shows 1.9 GeV points, the lower, 1.5 GeV points.

known as precisely as the samples with PMMA thicknesses of 1500 μm and below, and this imprecision may be the major contributor to the deviation of the experimental/theoretical power rations for these thickest PMMA samples.

As Figure 6 shows, when the NIST database is used instead of the Biggs database, there is a noticeably better agreement between theory and experiment with "new" ring values, and there is less dependence of the ($P_{expermental}$ / P_{LEX-D}) ratio on the filter type, and this ratio for most data, except for those obtained from measurements with the thickest PMMA + Al filter combination, is closer to unity.

This page intentionally left blank.

3. ABAQUS Modeling of the 3.3.1 Calorimetry Results

As described in Section 2 above, the temperature of the calorimeter block is monitored by a thermocouple imbedded in the back side of the block. All power calculations are made assuming that there is no variation in temperature throughout the block because of the high thermal diffusivity of aluminum. In reality there will be temperature variations throughout the block, and it is important to help assess the magnitudes of such variations. In order to help determine these temperature differences, computations using the thermal transient analysis, finite element program ABAQUS[8] were made. These calculations were done for two calorimetry runs – 1 each at 1.5 GeV and 1.9 GeV nominal ring energies. Only 254 μm of Be was used as beam filters-no additional aluminum filters were assumed. In each of these modeled runs, the temperature-time behavior of the calorimeter geometry used in the experimental runs 3/11/04 thru 4/14/2004 was calculated for heating by the X-rays for 117 seconds. These calculations correspond most closely to the two runs dated 4/14/2004 and labeled "a" (1.5 GeV nominal) and "f" (1.9 GeV nominal) in Appendix C below, or sequence number 1 in Table 2 above. LEX-D 7.56 with the "new" ring parameters was used to determine input power to the calorimeter block. In the calculations the effects of thermal conduction through the nylon support posts to the water-cooled baseplate and radiation to the baseplate (21 °C) and the interior scanner walls (25 C) were included.

Temperature contours in the calorimeter block were determined at discrete times after block heating started. The results for the 1.9 GeV case are shown in Figure 7 below at 19.3 seconds after X-ray beam heating of the beam plate started. The top panel shows the entire outline of the beamplate while the bottom panel shows a cross section through the center of the plate in order to help display the temperature-depth contours; note that there are grid elements outside the beam (upper panel). As the results show, the temperature in the front, center of the beamplate is predicted to be 32.56°C, while the edge of the plate is 31.77°C, a difference of 0.79°C. This same difference – about 0.79°C- was maintained during all times during the heating sequence. The temperature contour results for 1.5 GeV case are qualitatively similar to those of the 1.9 GeV case, except the effectively constant temperature difference between the center and edge positions was found to be about 0.16°C. Power deposition into the block as a function of depth was determined using the LEX-D code. The beam was assumed to have a rectangular outline the same as that measured and shown in Figure 4 – 10.5 mm x 90 mm. The outline of this beam is shown by the white, outlined box in the top panel of Figure 7.

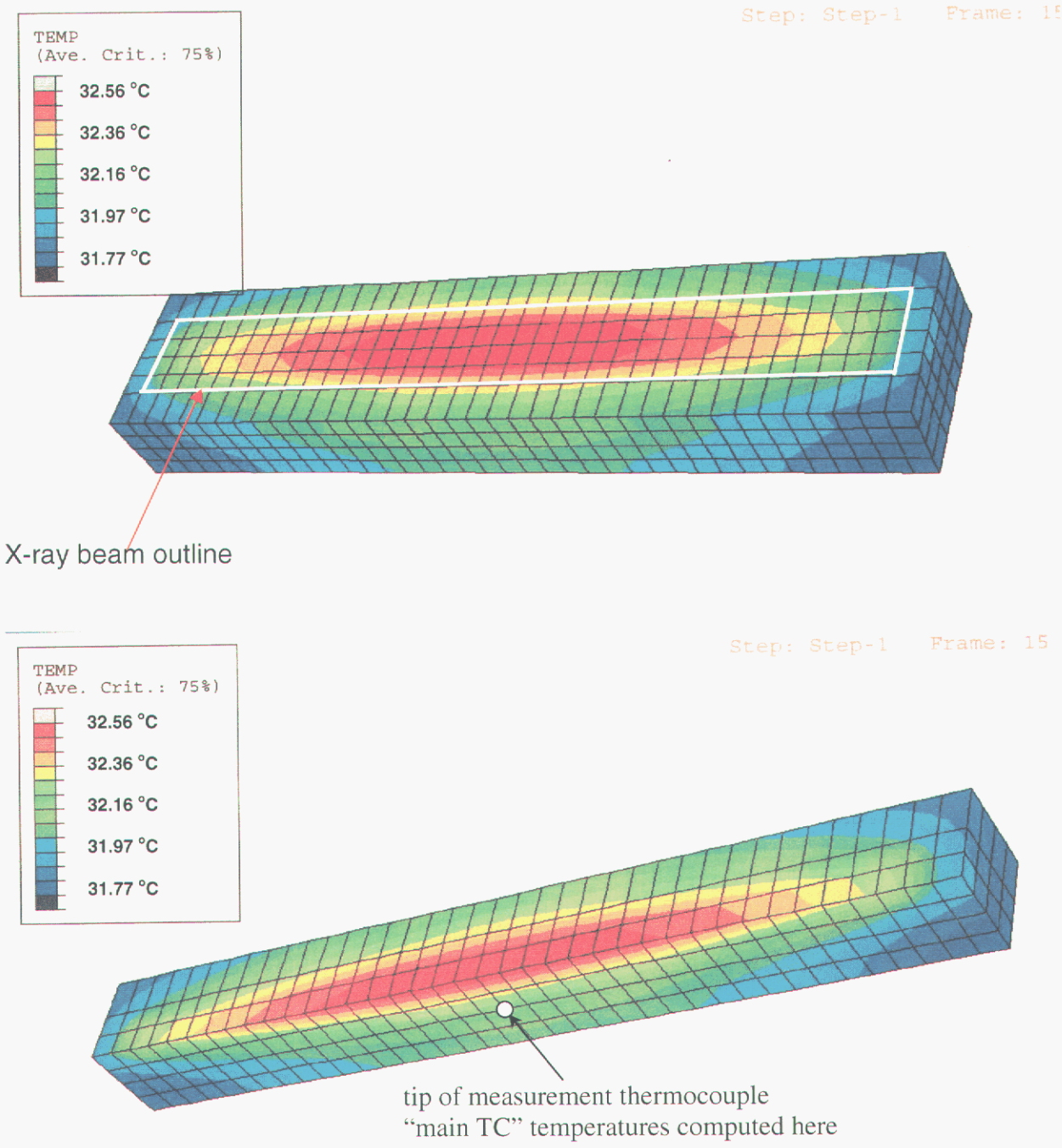

Figure 7. **Temperature contours computed with ABAQUS at 19.3 seconds into heating sequence by 1.9 GeV nominal X-ray beam. The top panel shows the contours for the complete block; the approximate outline of the beam is given by the white lines. The bottom panel gives the cross section through the center of the plate; it also shows the approximate location of the tip of the measurement thermocouple.**

These results demonstrate the differences in temperatures between the center of the beamplate, which is directly in the beam, and the outside of the plate. Although temperature contour plots such as shown in Figure 7 help in the visualization of the deviations from temperature uniformity in the plate, a quantitative measure of the validity of using one thermocouple measurement to characterize the temperature of the entire beamplate must be made. In addition, since the power input to the calorimeter is experimentally computed by using not the beamplate temperature, but rather its first time derivative (see section 2.2 above), it is important to assess how well the temperature derivative obtained from the thermocouple measurements represents the thermal response of the entire beamplate.

In order to help achieve these goals, ABAQUS was used to compute the average temperature of the beamplate as a function of time; this average temperature was then compared to the value of the temperature computed at the location of the thermocouple, at a position indicated in the lower panel of Figure 7. In the computations, the beam plate temperatures were computed at all positions ("nodes") in a 3-dimensional matrix with 7 nodes (beam plate height) x 5 nodes (beam plate thickness) x 39 nodes (beam plate width) simulating the beam plate. The average temperature as a function of time using these individual temperatures was computed and compared to the temperature-time behavior computed at the thermocouple position. The results of these calculations during the first ~110 s of heating are shown in Figure 8 for both the 1.5GeV (blue circles) and 1.9 GeV (red squares) cases. TC temperatures are plotted on the left ordinate. Average beamplate temperatures were also computed. The differences between the thermocouple position temperature and average block temperature are shown on the right hand ordinate of Figure 8. As the results show, after about 5 to 10 seconds, the differences between the temperatures are essentially negligible: there is about a 0.04°C difference in the 1.9 GeV case and a 0.008°C difference in the 1.5 GeV case. These very small differences at times greater than 10 seconds indicate that the rate of temperature change at the thermocouple position is the same as the rate of temperature change of the entire beamplate.

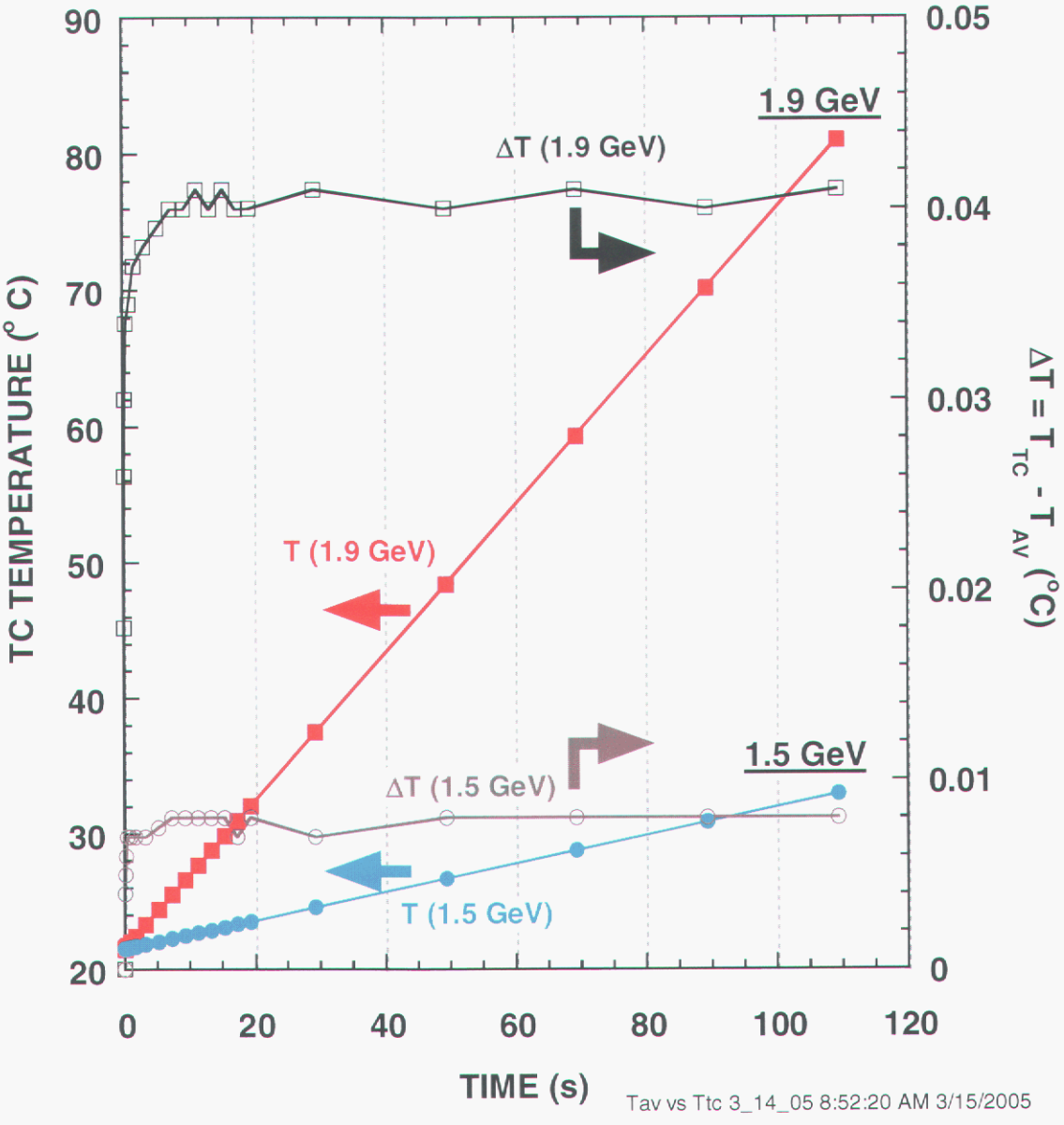

Figure 8. Temperatures computed with ABAQUS at the thermocouple (TC) position for heating during 1.9 GeV (red squares) and 1.5 GeV (blue circles) heating; temperatures are plotted on left ordinate. The right hand ordinate shows the differences between the TC position and the average block temperature.

An estimate of the percentage error in calculated powers resulting from the assumption that the thermocouple rate in change of temperature represents the average temperature rate of change of the beamplate can be computed by the following expression:

$$(4)\quad E(\%) \sim 100 \cdot \frac{(dT_{TC}/dt - dT_{AV}/dt)}{\langle dT_{TC}/dt \rangle} = 100 \cdot \frac{d(\Delta T)/dt\mu}{\langle dT_{TC}/dt \rangle}$$

Where,

$E(\%)$	=	the percentage error in the power calculation using the TC temperature to represent the temperature of the entire beamplate
dT_{TC}/dt	=	the rate of change in temperature at the TC position;
dT_{AV}/dt	=	the rate of change in the average temperature of the entire beamplate
$\langle dT_{TC}/dt \rangle$	=	the average rate of change of the TC temperature (average slope of the T vs. time characteristics).

Linear fits to the temperature vs. time behaviors of both the 1.9 GeV and 1.5 GeV beam heating simulations were made to determine $\langle dT_{TC}/dt \rangle$ values. In addition, a two exponential curve fit to the ΔT values were also made; these fits were differentiated to determine $d(\Delta T)/dt$. Using these fits and equation (4), it was found that the value of E(%) was less than 0.2% after 2 seconds of heating by either the 1.5 GeV or the 1.9 GeV beams. These results indicate that the rate of temperature change recorded by the thermocouple is indeed a good indication of the rate of change in the temperature in the entire block and support the use of the thermocouple to accurately determine beam powers.

As described in the beginning of this section, the primary intent of the ABAQUS calculations was to help assess the magnitude of the temperature differences in the calorimeter block during X-ray beam heating. From the calculated temperature-time results shown in Figure 8 above, the predicted temperature rises (dT/dt) computed by ABAQUS can also be compared to the experimental data. These results are given in Table 3 below.

TABLE 3. Comparison of Experimental vs. ABAQUS results for the modeled heating.

Energy for (dT/dt) – [°C/s]	Experiment	ABAQUS	Experiment/ABAQUS
1.5 GeV	0.105	0.114	1.09
1.9 GeV	0.579	0.556	1.04

As the results show, there is good agreement between the ABAQUS-determined values and the experimental ones; it is likely that even better agreement would result if a finer geometric mesh were used to model the beamplate. However, as indicated above, the intent of using ABAQUS was to help assess the approximate magnitude of temperature variations in the beamplate, and the results of Table 3 confirm that the approach taken was more than adequate.

This page intentionally left blank.

4. Calorimetry Studies at the Advanced Photon Source

4.1 Introduction and experimental arrangement

At the Advanced Photon Source (APS), Argonne National Laboratories, Argonne, Illinois, Beamline 10-BM has been used to perform LIGA exposures. In order to provide a spectrum useful for LIGA exposures, this beamline contains a single, platinum-coated mirror. This mirror acts somewhat like a low pass filter, effectively decreasing the average photon energy, or "softening" the spectrum of the photons emitted from the 7 GeV APS synchrotron. Figure 9 below is a simplified sketch of some of the major components of the beamline near the LIGA linear stage scanner. The angle of the mirror shown in the figure can be varied from about 6 mrad to 9 mrad; initial angles when exposing LIGA samples mounted on the scanner have been around 8 mrad. The Be window chamber is an enclosure through which helium gas flows in order to help minimize any oxidation of the beryllium window located on the output of the mirror tank; the entrance to this small chamber is a Be window, while the exit window is 25 μm

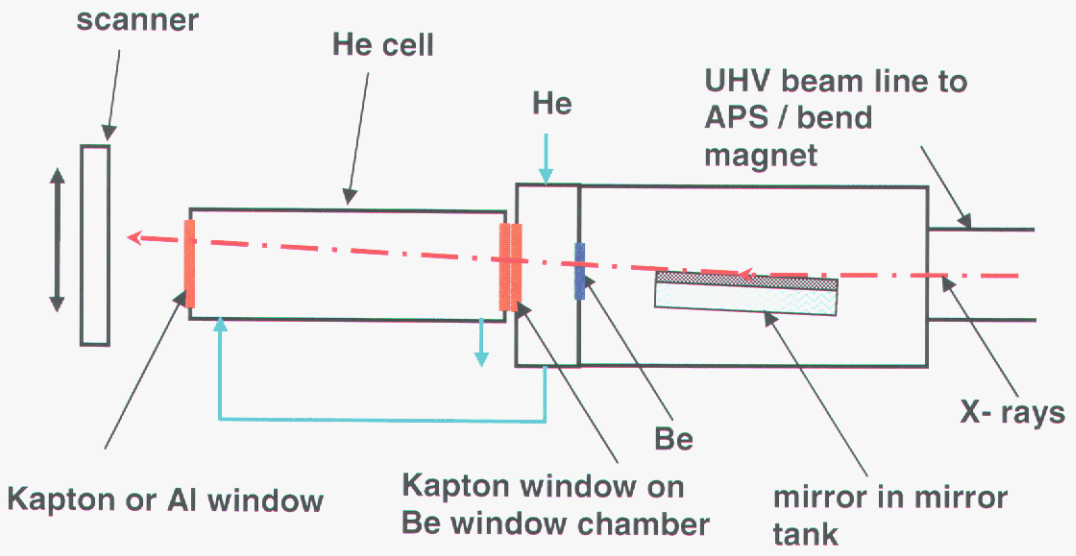

Figure 9. Simplified Schematic of APS 10 BM Beamline near the scanner

thick Kapton; the distance between the Be window and the Kapton window is about 1 cm. After exiting the Kapton window, the X-rays go through a helium cell (~0.5 m long). The helium exiting the Be window chamber can be flowed through this cell in order to help minimize ozone production in the hutch where the scanner is located. The right hand (upstream) end of the cell could be open (in which case it is pushed against the window chamber) or closed with loosely fitting Kapton (25 μm thick). The left hand side (downstream) is sealed with either aluminum foil (10 μm thick) or Kapton (25 μm thick). After exiting the downstream side of the He cell the X-rays traverse about 10 cm of air before striking the scanner stage (sample area).

Photographs of the same region depicted in Figure 9 near the end of the beamline and the calorimeter used to measure the beam power are shown in Figures 10 and 11, respectively.

Codes such as LEX-D can predict the reflected power when using a mirror in a synchrotron bend magnet beamline. However, such beamlines typically are composed of several elements, each of which can affect beam power. In addition, parameters such as mirror angle, surface roughness and coating material must be precisely known in order for the LEX-D predictions to be valid. For these reasons, it is important to have an independent experimental check of this power delivered to the scanner stage where the LIGA samples are mounted. An initial measurement of the total X-ray power at the sample position was therefore made.

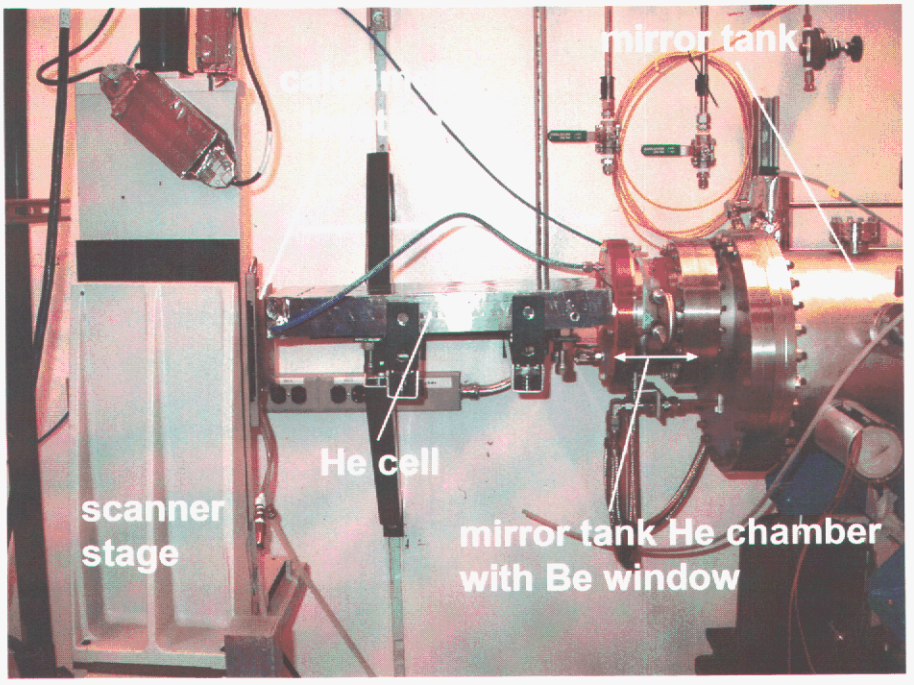

Figure 10. Photograph showing 10-BM beamline near scanner stage

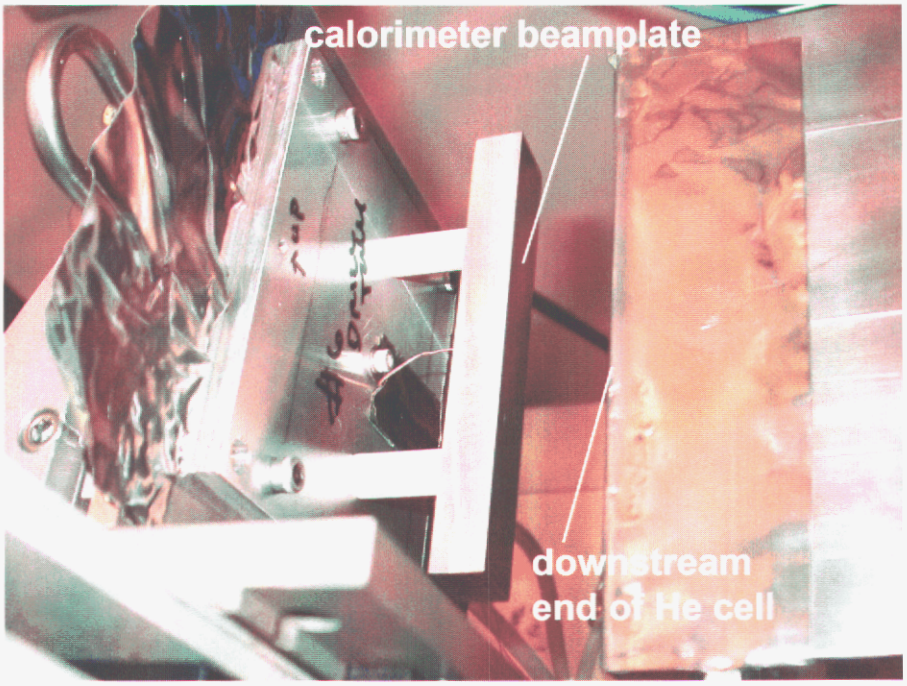

Figure 11. Photograph showing a calorimeter mounted on scanner stage for power measurements.

The calorimeters used in these tests were similar in design to those used in the ALS calorimetry work described in Section 2 above. However, the calorimeter beam block was machined to be wider in order to accommodate the wider APS beam. In addition, two aluminum calorimeter blocks were made: One (1.27 cm thick) was used to measure the power reflected from the mirror, while a second, 3.8 cm thick calorimeter was used to measure the power of the direct beam. As in the case of the ALS work, calorimeter blocks were fabricated from aluminum to help minimize power loss due to fluorescence radiation while maintaining good thermal responsivity. LEX-D calculations indicate that the power loss when the thinner calorimeter was used with the Pt mirror (angles between 6 mrad to 9 mrad) should be less than 0.05%. Similar predictions for the thicker calorimeter indicate losses in the direct beam to be no more than about 1.4%.

When these first calorimetry measurements runs were performed, final alignment of all apertures and beam limiting surfaces in the beamline had not been completed. As a consequence, not all the beam was passed through the beamline unobstructed. Figure 12 shows an image of the direct beam, taken with X-ray sensitive film of the direct beam taken at the scanner position on 6/30/04.

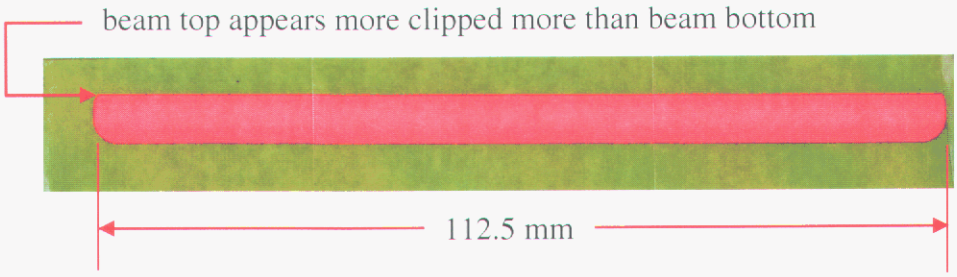

Figure 12. APS direct beam image on X-ray sensitive film of APS direct beam onto calorimeter surface.

As this film shows, both the upper and bottom portions of the beam appear clipped, with the upper portion of the beam clipped more than the bottom. Although the highest energy portion of the beam was transmitted, it is likely that a few percent of the beam power was being lost at the time that our measurements were taken. In the LEX-D calculations an unobstructed passage of the beam after the axially symmetric limiting apertures in the beam at the front end of the beamline is assumed. This was apparently not the case at the time of the measurements, and this factor alone should make LEX-D predictions higher than the results of any experimental measurements. The X-rays in the central, horizontal portion of the beam have average energies higher than those at the upper and lower beam positions, those positions which were evidently clipped in the beam. However, there can be significant amounts of power in these beam portions.

4.2 Results

The first calorimetry data taken at the APS involved setup and operational verification of the calorimetry system. In these initial tests the 1.27 cm thick calorimeter was used and the beamline mirror was kept at a fixed angle of 7 mrad. During all calorimetry measurements the APS was running in "top-off" mode, where the electron ring current stays constant at 102.0 +/- 0.2 mA. X-ray sensitive film indicated a beam width on the calorimeter of 109 mm.

Although this calorimetry setup step was expected only to be a routine procedure, the results proved otherwise. The temperature-time data for this initial series of steps are shown in Figure 13. In this graph, calorimetry results from three different test conditions are plotted and the time scales from each test are offset shifted so that the heating start times for the calorimeter block approximately coincide.

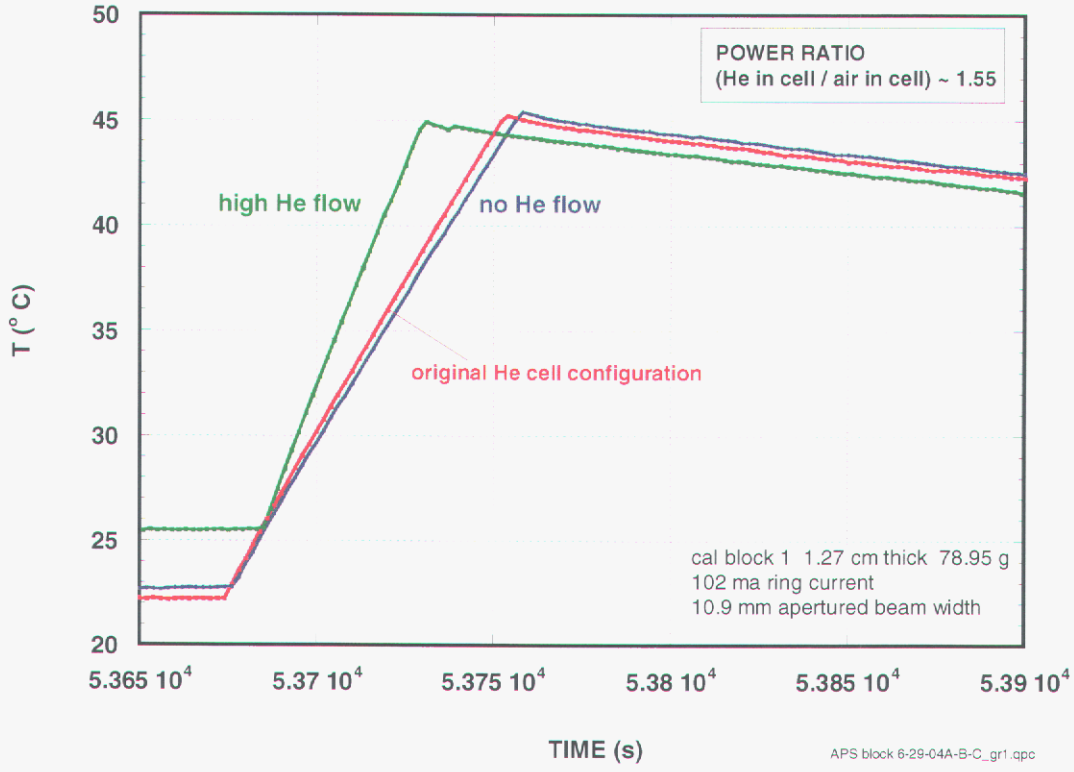

Figure 13. **Initial temperature-time data acquired during calorimetry system Setup at 10-BM, APS.**

The red trace in Figure 13 shows the calorimeter response with the beamline in the "as-received" condition; that is, with original He cell configuration, where the window on the left hand (downstream) side of the He cell (see Figs. 9 and 10 above) was 10 μm of Al and the right hand (upstream) end of the cell had no seal, but was pushed against the left hand surface of the Be window cell. He was flowing through this Be cell and into and out of the He cell on the exit of the mirror tank (see Figure 9). Calculations using LEX-D indicated that there should be substantially more power incident on the calorimeter than measured if the He cell had been filled with He. Since it was reasonable that the cell may not have had He, but rather air, the He flow to the cell was intentionally stopped, the cell flushed with air, and the calorimetry measurement repeated. The data indicated by the blue trace in Figure 13 resulted; since the power is proportion to the slope the temperature-time calorimeter plotting during beam heating, these results showed that indeed the He cell, "as-received" was likely filled with a mixture of more air than He since the heating curves for these two cases were nearly identical. To further investigate this possibility, the right hand (upstream) end of the He cell was taped with Kapton tape so as to form a tighter seal than originally possible with no tape. Then the He flow through the He cell was reinstated for about a half hour; a beam power measurement was again taken, and the results are shown by the green curve in Figure 13. The computed ratio of powers for the cases of (He in the cell / air in the cell) was about 1.55, demonstrating the sensitivity of the total power delivered to the calorimeter on the He cell composition. These results underscored the necessity of

good beamline characterization and the utility of calorimetry (or some other total power technique) to helping achieve this characterization. In the work at the APS, the calorimetry resulted directly in improvements made to the He cell. In addition, the results also demonstrate the need to maintain constant environmental conditions in the beamline so that sample dose depositions can be reliably computed using LEX-D.

Using the He cell with a better seal and with helium flowing in the cell, the power delivered to the calorimeter was measured as a function of mirror angle. The results were compared to LEX-D predictions, and the ratio of the experimentally measured powers to those predicted by LEX-D are shown in Figure 14. Time limitations at the beamline restricted the number of possible measurements, but the results show that power delivered varied from about 78% (9 mrad mirror) to about 86% (6 mrad mirror) of that theoretically predicted. Note that at 7.5 mrad aluminum filters with two different thicknesses (25.6 μm and 51.2 μm) were installed in the beam path; the experimental/theoretical power ratios are also plotted in this figure as a blue datum and green datum, respectively. Note that the power ratio delivered at 9 mrad was less than that at 6 mrad, and may reflect the increased influence of small levels of air contamination in the He cell on the softer, 6 mrad spectrum. The exact reasons for the differences between experiment and theory in these measurements were not known at the time the data were taken. The original intent of the measurements was to determine whether the power delivered to the scanner was within a factor of two of that expected from LEX-D predictions, and not to perform an accurate calorimetric assessment of beam power. Only with better beamline setup and characterization (including, but not limited to, factors such as an unobstructed beam, He cell gas composition, and accurate knowledge of mirror angles) can a precise comparison of theory with experiment be made.

In a separate measurement experiment using the thicker calorimeter, the direct beam power was measured. When taking these calorimetry data it was necessary to remove the He cell since the larger calorimeter block did not fit in the space available between the scanner stage and the left hand (downstream) side of the He cell. The results of these measurements indicated a ratio between the measured and LEX-D predicted powers of about 91%. As indicated in the section above, the delivered beam was apparently clipped on its top (Figure 12 above), so not all the available power was delivered to the calorimeter. In addition, thermal diffusion in the thick aluminum block used to measure direct beam power might also lower detected powers (see below).

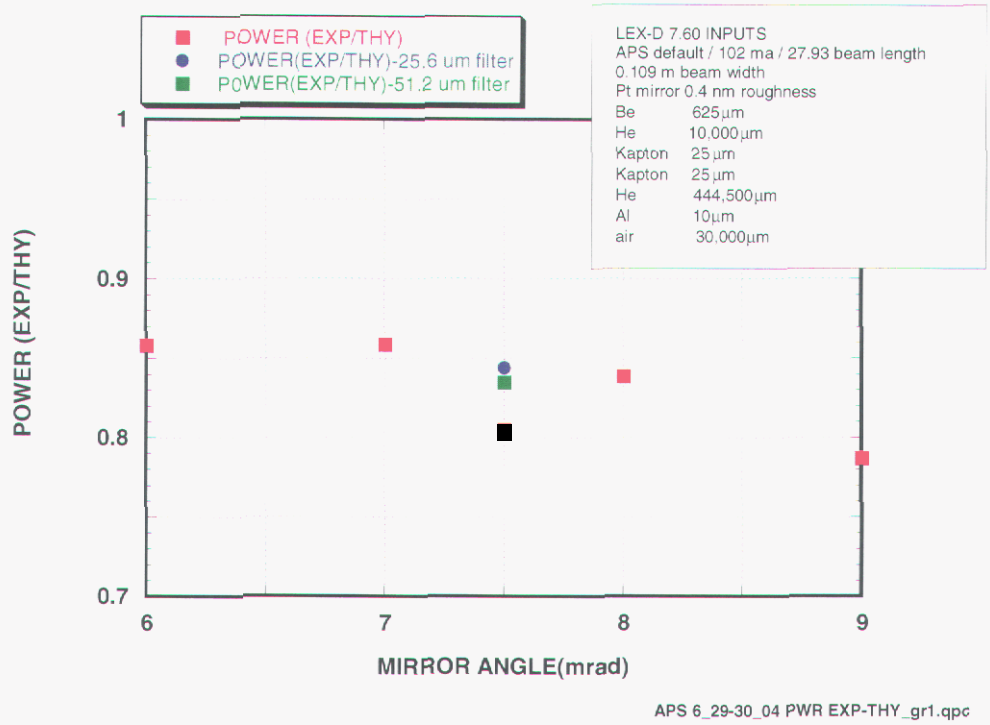

Figure 14. **Ratio of experimentally measured power / predicted (LEX-D) power as a function of mirror angle.**

Since all LEX-D calculations were performed assuming no clipping was occurring, it may be likely that the measured power ratios might be as much as 9% higher than shown, and may vary from about 95% (6 mrad) to 87% (9 mrad). Before precise measurements of these power ratios can be made, beam clipping must be eliminated and proper He cell operation must be established. However, these measurements demonstrated the utility of calorimetry in determining proper beamline operation and calibration. Further applications of calorimetry at the APS would also benefit from ABAQUS modeling of the temperature variations and responses of the aluminum blocks which were used at APS. The beam plates were significantly thicker than those used at the ALS, and it would be important to determine if thermal diffusivity in the blocks was limiting the measurement accuracy.

This page intentionally left blank.

5. Other Methods to Determine Beam Power

5.1 Motivation

The results of the initial calorimetry work done at the APS show the utility of using calorimetry to help determine proper beamline operation. Although performing calorimetry is a simple technique, it does require data acquisition by a computer and analysis of the temperature-time results. It would be convenient and desirable to have other methods of determining beam power which would not only be simple, but have essentially real-time, direct readouts of X-ray power. Such methods could be used not only in Sandia LIGA's prototyping beamlines located at the ALS and Stanford Synchrotron Radiation Laboratory (SSRL), but also at the APS, where such a beam power monitor could be one means of helping to promote process control in the synchrotron exposures. Moreover, when using a calorimeter, the practical issues of staying below a maximum calorimeter temperature and requiring cooling the calorimeter to an initial, essentially constant temperature prior to power readings make the use of a calorimeter for repeated, nearly constant power monitoring impractical. Thus, aside from these infrequent samplings of power, the use of some device other than a simple calorimeter could offer some practical, operational advantages.

As a starting point, properties of such direct-reading power monitors could include the following:

1. Direct, repeatable, essentially real-time output proportional to total X-ray power;
2. Output proportional to total X-ray beam power only –X-ray spectrum independent;
3. Useable at APS (with mirror), ALS and SSRL (with mirror or chopper);
4. Calibration traceable to calorimetry;
5. Potential power accuracies of +/- 10% or better;
6. Simple, small, low cost- no computer required, few parts;
7. Robust – endure X-ray environment.

In order to help develop such power monitors, some initial experiments were performed to evaluate some potential devices as power monitors. Other devices and techniques undoubtedly exist, and the current work should be viewed only as one starting point for development of power meters. In the initial tests described below, no long-term testing (property 7 in the above list) was performed. Therefore, as a follow-on study, the "survivability" of any new power monitoring device to extended X-ray irradiation must be demonstrated. These long-term tests are beyond the intended scope of the current work.

5.2 Description of the devices

In this initial evaluation three devices were built and tested and their responses compared to calorimetry:

1. A photodiode;
2. Heat flux sensors; and
3. A calorimeter variant.

The photodiode tested was model FDS-100 purchased from ThorLabs and chosen because of its low cost, sensor area (~4 mm x 4 mm) and small, overall packaging size (on a TO-5 header). Before using the photodiode to monitor power, the clear window in the stock photodiode was removed to eliminate X-ray absorption in the window. The photodiodes were used in either a "direct" mode, with X-rays directly incident (through an aluminum filter) onto the sensor area, or in an "indirect" mode, where the incident X-rays first hit a target and the photodiode was used to detect the secondary radiation (fluorescent photons) emitted from the target. The photodiode was used in an unbiased mode in all work; the photodiode current was measured with a picoammeter (Keithley 487) and the analog output used for data acquisition in these tests. Figure 15 shows a photodiode used in an indirect configuration, with 0.50 mm of Ti as the target for the incident X-rays. Copper has also been used as a target. The active area of the photodiode, just barely visible in the photograph, faces a sheet of titanium, which is oriented at approximately 45° to both the incident X-rays and the photodiode.

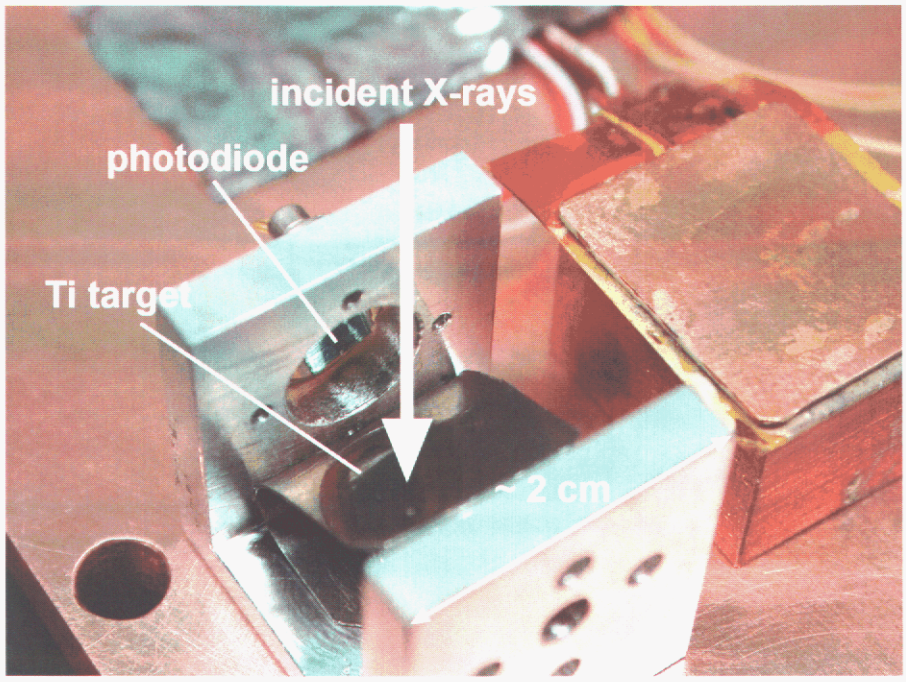

Figure 15. Photodiode used in indirect mode to detect incident X-rays.

Heat flux sensors are available from several different companies (Vatell, Omega, RdF) and are all differential thermocouple arrays. One array of thermocouples is placed on each side of a thin, insulating layer (typically polyimide), an arrangement used to detect heat flow perpendicular to the device. Such sensors are used primarily to detect radiant heat flux, and the difference in temperature across the insulating layer results in a voltage output proportional to the heat flux through the layer. Multiple thermocouples are used in the array on each side of the polyimide layer in order to increase the signal. In the current work, in order to use the device as a monitor of X-ray power the sensor is sandwiched with epoxy between two metallic layers – a top layer, which converts the X-ray power into heat, and a bottom metallic block which conducts the heat to a water-cooled heat sink. Heat flows from the top layer through the sensor to the bottom heat sink; the sensor produces a voltage output proportional to the heat flux. Figure 16 shows such an arrangement. Choosing the material and thickness of the top absorber layer is a tradeoff between absorbing the majority of the incident X-ray photons (thicker layers better) while maintaining a relatively fast response (thinner layers are better). In practice, it would be desirable to absorb >99% of incident X-ray power in the top layer. In addition, the projected area of the heat flux sensor should be a good match to the X-ray beam height in order that the heat flux through the sensor is maximized. In practice, the voltage output of the heat flux sensor would be calibrated against a calorimeter.

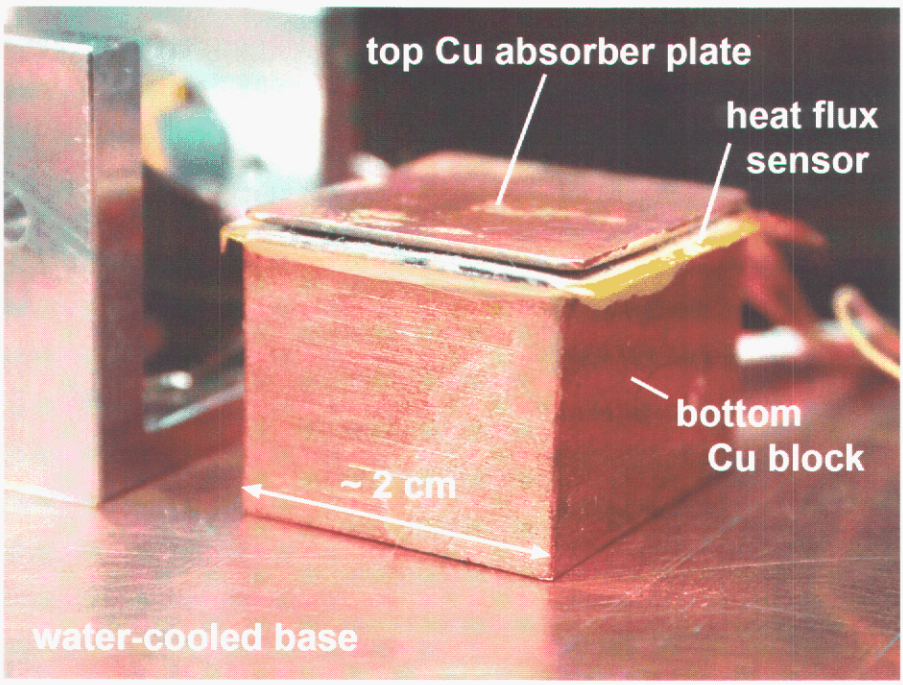

Figure 16. Heat flux sensor arrangement for X-ray power measurement.

The third device which was built and tested was a variation of a standard calorimeter. This is basically a calorimeter block which is not thermally isolated from a cooling

substrate, such as using nylon standoffs (see Figure 3 above), but has a relatively large thermal conductance to the cooling substrate. With X-ray power input, the temperature of such a device would initially increase linearly with time, similar to a regular calorimeter. However, because of the appreciable, or strong, thermal link to the cooled substrate, the temperature of the device should, in principle, reach a steady state temperature determined primarily by the power balance between incident, input X-ray power, and thermal conduction losses. The difference in temperature between this steady state block temperature and the base temperature should be proportional to the input power. The challenge in creating a successful device based on this "strong thermal conductance link" concept is making the response time as short as possible consistent with having accurately measurable temperature differences. The thermal response time of such a system should be proportional to the inverse of the conductance of the thermal link formed by the legs connecting the top block to the water-cooled substrate base. However, the steady state temperature reached in the top block should also be inversely proportional to the same conductance. Thus, there is a tradeoff between the magnitude of the steady state temperature change and the response time – a device with a short response time also produces a small increase in temperature, which could make accurate measurements of power difficult. A photograph of such a device is shown in Figure 17. A thermocouple, not visible in this photograph, is glued into the top aluminum block with heat conductive epoxy.

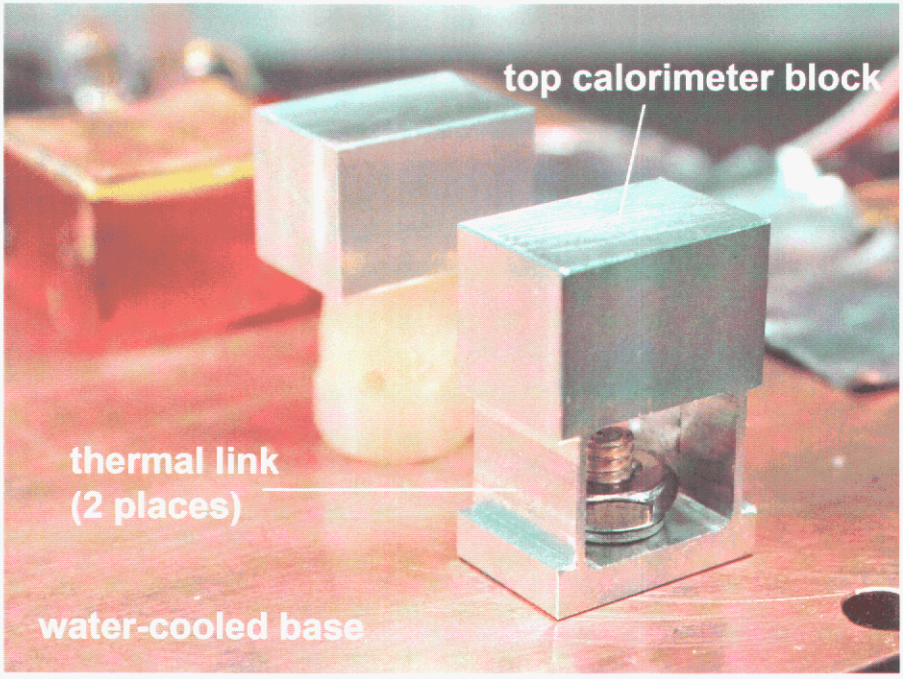

Figure 17. Thermally linked calorimeter; a conventional calorimeter design is in the background.

The response to X-ray input of each of these three devices (heat flux monitor, indirect photodiode, linked calorimeter) were compared to that of a conventional, thermally

isolated calorimeter. The calorimeter block in this case was made of aluminum with dimensions of 15.2 mm high x 10.2 mm wide x 10.2 mm thick and isolated from a mounting plate with a modified nylon standoff similar to that used in the calorimeter described in Section 2 above.

In the case of the conventional and linked calorimeters, type K thermocouple outputs were recorded. The thermocouple outputs, voltage output of the heat flux monitor and the current produced by the photodiode (amplified by a Keithley 487 picoammeter) were all measured simultaneously during X-ray beam irradiation. The experimental arrangement is shown in Figure 18. The incident X-ray beam illuminates a rectangular area across the top shield plate, which acts as a mask, used to sample different areas of the same beam. Since all devices were located at least 5 mm away from the end of the X-ray pattern, the flux striking each device should be the same (within <0.5% because of beam divergence). As the figure shows, a copper, top shield plate (~3.8 mm thick) with four apertures defines the extent of the X-ray irradiation of each device: In the case of the heat flux monitor and calorimeters, there is a 7.62 mm wide window; in the case of the photodiode assembly, a there is an 2.58 mm diameter hole. The base of this entire assembly is mounted onto the water-cooled sample block in the vacuum scanner on beamline 3.3.1. The influence of any secondary radiation produced by the sidewalls in the shield plate apertures should be negligible in these experiments since the amount of secondary power (calculated by LEX-D) was less than 10% of the expected incident power and, because of solid angle considerations, significantly less than 10% of this power (<1% of total input power) could reach the different detector devices located under the top shield plate.

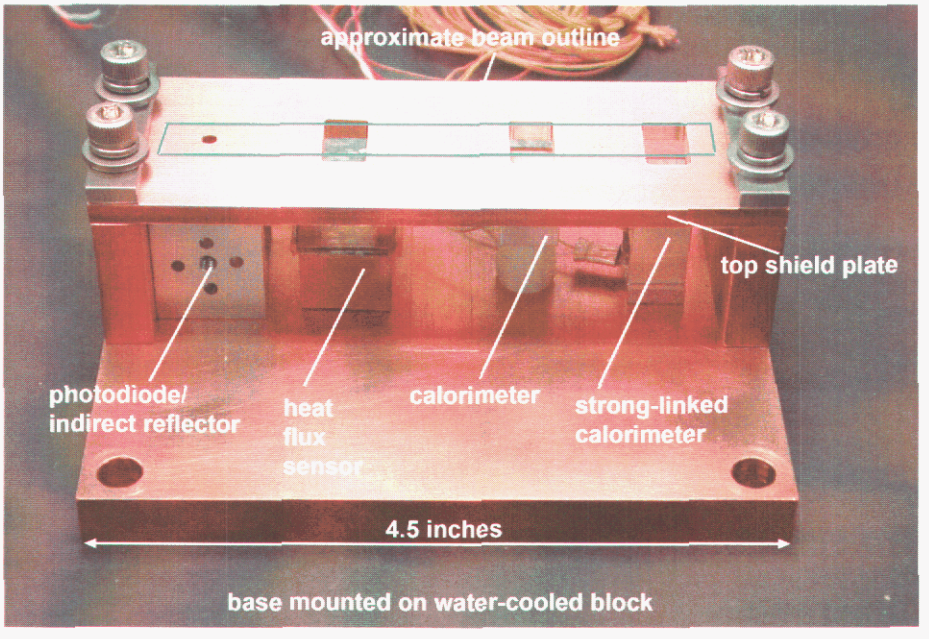

Figure 18. Experimental arrangement for measuring power device outputs.

5.3 Results

Figure 19 below shows typical output responses from the four devices in the experimental arrangement of Figure 18: The temperatures of the calorimeter, linked calorimeter (called "S-calorimeter" in the Figure, and linked calorimeter base are given by the left-hand scale, while the outputs of the photodiode (with Ti target) and heat flux sensor are given by the right-hand scale. Note that the output of the heat flux sensor has been multiplied by 10 in this figure. The photodiode output was amplified by a picoammeter and converted to a voltage (10^4 volts/amp gain). During this particular sequence, the X-ray beam was on from about 0 seconds to 46 seconds.

As the results show, the detector with the fastest response is the photodiode system. This rapid response, simplicity, and relatively low cost are attractive features of using the photodiode system as an X-ray power meter. However, the photodiode system has one major drawback as a total power meter – its output depends on the incident X-ray spectrum. When the photodiode is used either with the beam directly incident upon its active surface or with the beam incident on a secondary surface as was the case in the current test setup (Figure 18 above and description), the photodiode output is not proportional to the total, incident X-ray power.

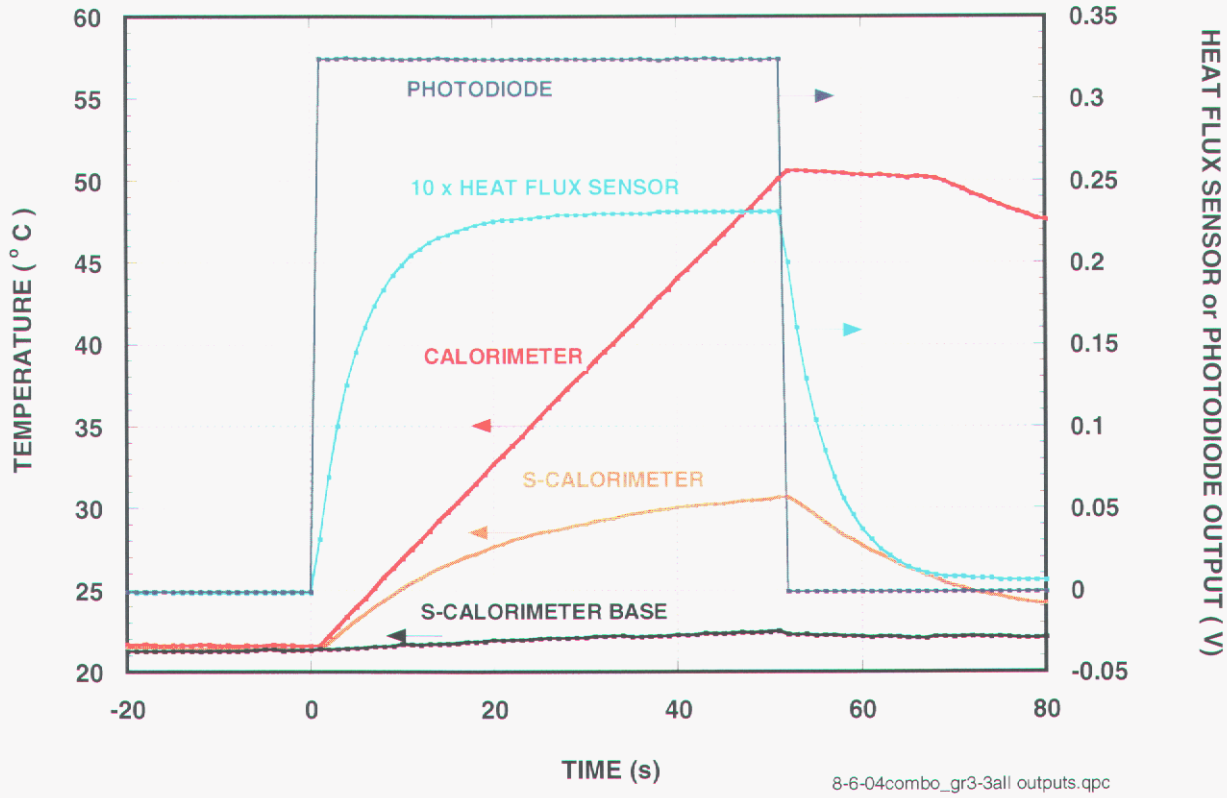

Figure 19. Comparison of typical outputs from photodiode, heat flux sensor, and two types of calorimeters during x-ray irradiation

In order to demonstrate this dependence on the spectrum, aluminum filters of different thickness were put in the beam in front of the photodiode to determine the relationship between the photodiode (PD) output and the measured input power. Aluminum filter

thicknesses included 5.6 μm, 25.6 μm, 38.8 μm, 57 μm, 115.9 μm and 205.6 μm. All thicknesses were computed using measurements of foil areas and aluminum filter foil masses, and using the aluminum density (2.7 g/cm^3). Figure 20 shows spectra for these Al filter thickness (ALS nominal 1.9 GeV, 320 mA ring current) predicted by LEX-D. As expected, with increasing Al thickness, for a given ring current, not only is the total power reduced, but the X-ray spectrum is hardened.

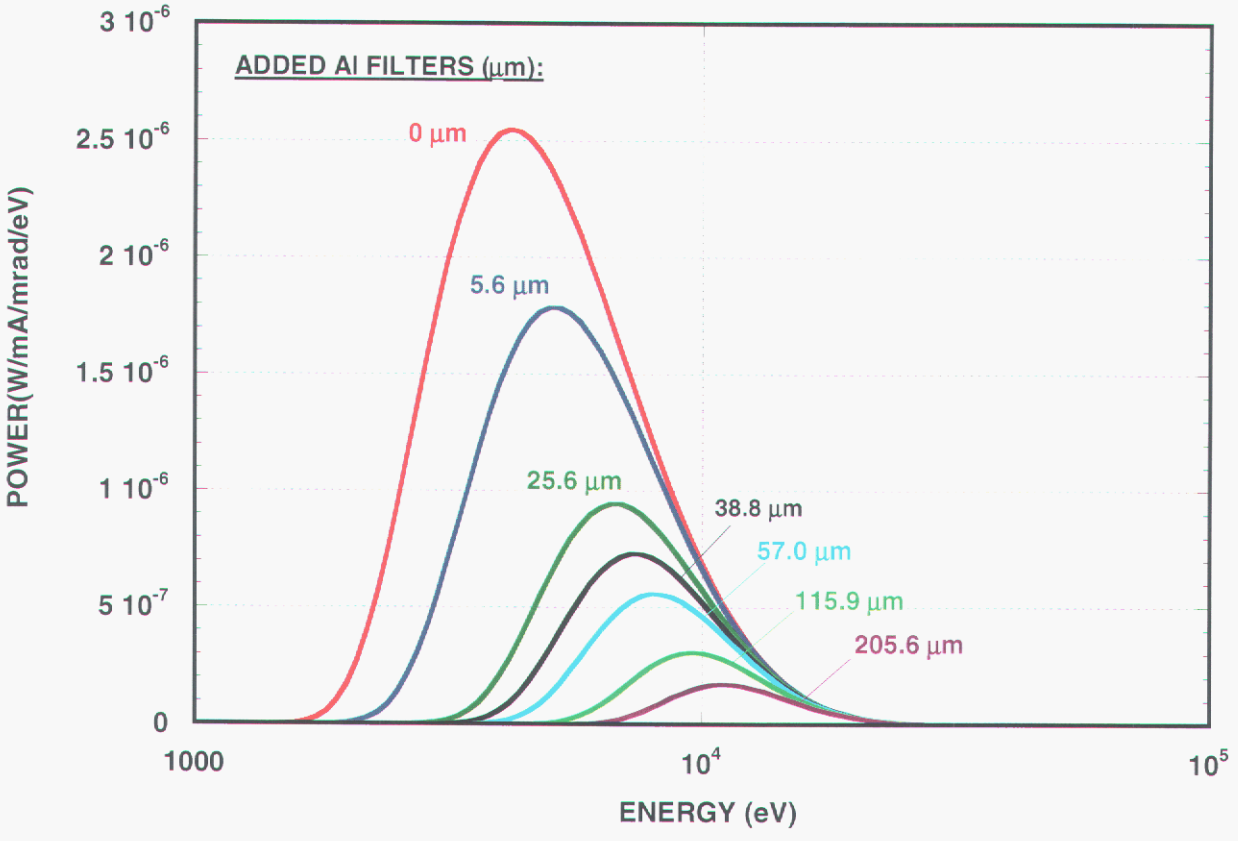

Figure 20. **X-ray spectra predicted for ALS operating at 1.90 GeV nominal, 320 mA using LEX-D. The thickness of the aluminum filter used (in addition to 254 μm Be) is given next to each curve.**

The dependence of the PD output with differing spectra is demonstrated with data which are shown in Figure 21. In the upper frame in Figure 21 the photodiode output using a photodiode setup similar shown in Figure 17 (PD operating in an "indirect" mode, copper target or "backstop") is plotted as a function of the total, incident power measured by the "regular" calorimeter (see Figures 17 and 18 above). The original motivation for using a target was to eliminate high power loading on the PD due an incident X-ray beam. The outputs versus total power for different aluminum filters are made explicit in Figure 21a by plotting data taken with the same thickness aluminum filter with the same color line and symbols. As the data show in Figure 21a, for each filter thickness the PD output is proportional to the input power. The input varied as the beam power varied. However, with thicker aluminum filters, which progressively hardened the input spectrum, the PD output dependence on the power input changed.

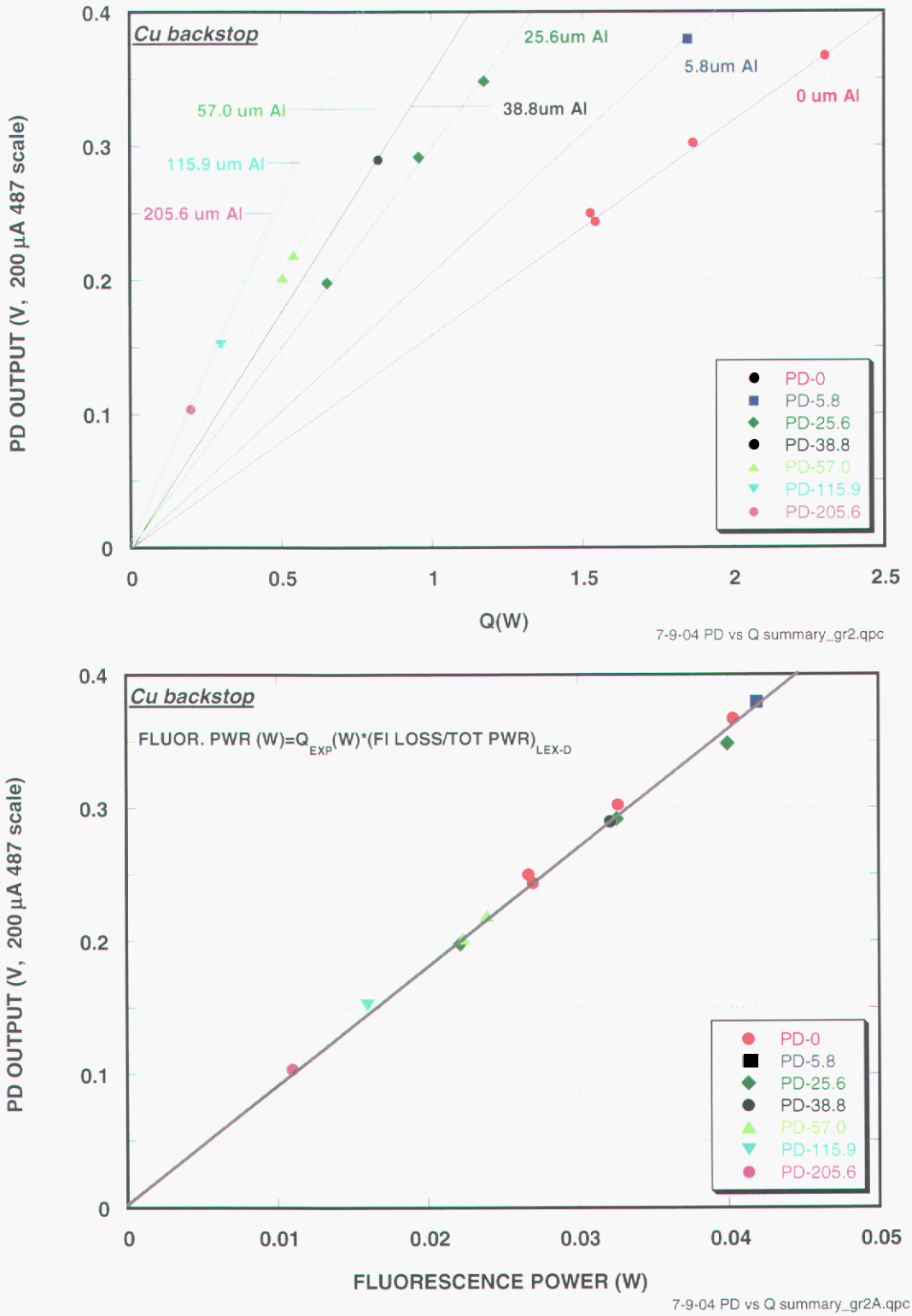

Figure 21. **The upper frame shows the PD output versus input power for different aluminum filter thicknesses. The lower frame shows the same PD outputs versus predicted, total fluorescence powers.**

Since the fluorescent power reradiated from any material irradiated with X-rays is influenced by changes in the input X-ray spectrum, the data in the upper frame of Figure 21 can be corrected for fluorescent yield effects by multiplying the experimentally measured input power by the ratio of the (fluorescence power / input power) computed using LEX-D. The results of this normalization are shown in the lower frame of Figure 21, where the PD output is now plotted versus fluorescence power reradiated by the copper target. As these data show, there is a now a good proportionality between the PD output and the total fluorescence power. Similar behavior was observed when using a titanium target – that is, there was a direct relationship between the PD output and the total fluorescence power radiated from the titanium target as predicted by LEX-D. Thus, when using a photodiode in the indirect mode, the fluorescence yield dependence of the target material results in a dependence of the PD output on the input spectrum. This is undesirable for a total power measurement, where device output should be independent of the spectrum. In retrospect, choices of elements or materials with lower K-shell binding energies than the Cu (~9 keV) or Ti (~5 keV) might have provided a more linear behavior of the PD output with total input by having fluorescence energies substantially lower than the ~4 keV peak energy in the unfiltered ALS spectrum. For instance, Al (K_α~1.6 keV) and Si (K_α~1.8 keV) are examples of practical materials which have lower binding energies and might provide such an improvement. In future work on PD-based power meters, such materials will be tried as "backstop" materials.

A dependence on the X-ray spectra was also observed when a photodiode was used to detect incident X-ray power in a different configuration, a "direct" mode. In this configuration the incident X-ray beam hit the active area of the photodiode after passing through an aluminum filter. This filter, which was necessary to reduce the incident power of the beam so as not to destroy the photodiode, was also made of aluminum and was 600 μm thick. This was approximately the thinnest aluminum which could be used with the picoammeter / photodiode combination without overloading the picoammeter. The response of the photodiode to differing input powers, created by using the same ensemble of filters (in addition to the 600 μm thick filter) as used to test the "indirect" photodiode arrangement is shown in Figure 22 below.

The experimental arrangement shown in Figure 18 above was used and the output of the heat flux meter was also measured. In Figure 22, the response of the photodiode is plotted on the left-hand vertical axis with solid symbols, while the response of the heat flux meter was plotted on the right-hand vertical axis with open symbols; both responses are plotted versus the experimentally measured power on the apparatus calorimeter. As these results show, the photodiode output does not vary linearly with X-ray input power when additional aluminum filtering is used to decrease the power. These results, as in the case of the "indirect" photodiode arrangement, show that the output of the photodiode is dependent on the input X-ray spectrum.

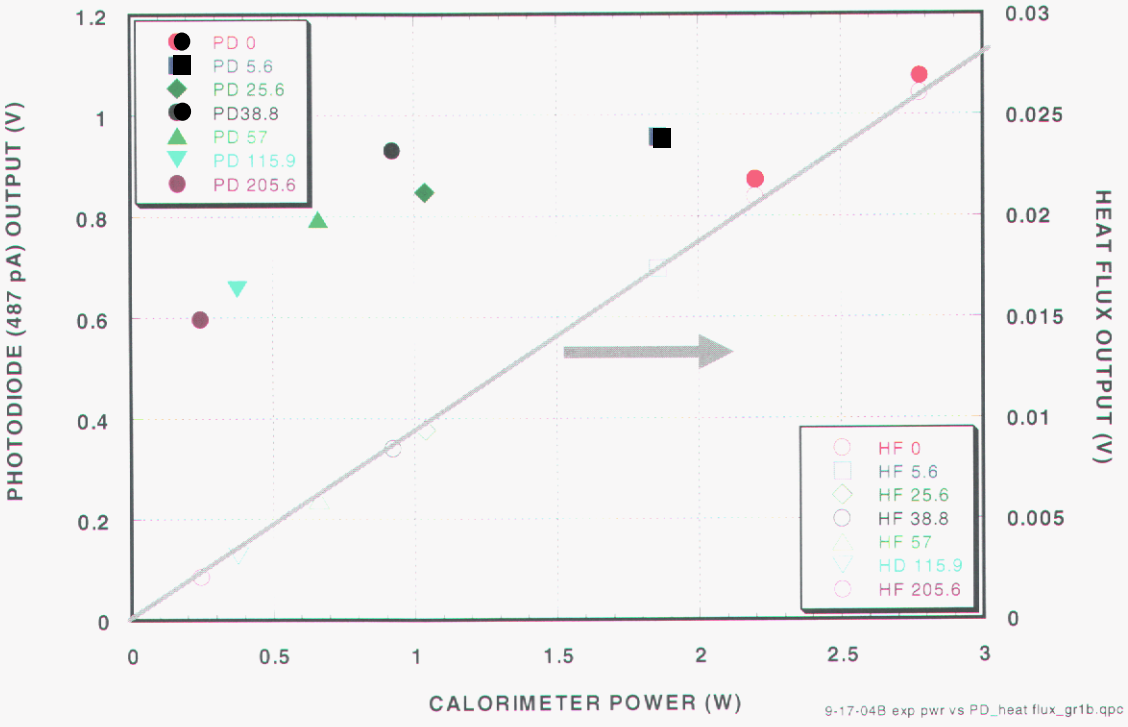

Figure 22. **Photodiode (solid symbols) and heat flux monitor (open symbols) responses to X-ray input. PD used in "direct" mode operation with a 600 µm thick Al inline filter; additional filter thicknesses are given in the plot legends.**

Compared with photodiodes, the heat flux sensor-based systems have a relatively slow response, with a response time (µ) of about 5 s. About 15-20 seconds are required to reach a steady state output which is proportional to the input power. Unlike the photodiode system, however, these heat flux sensors have outputs independent of the X-ray spectrum. This is shown in Figure 23 below, which shows the output of one heat flux sensor versus input power; this plot is similar to the PD plot shown in 21a above with the differently colored and shaped data points corresponding to different aluminum filter thicknesses used in the incident X-ray beam. As the results in Figure 23 show, there is a linear dependence of the heat sensor output (taken in steady state) versus input power. Heat flux monitors from two different manufacturers (RdF and Omega) were tested and both monitors had linear output/X-ray input characteristics. Reducing the response time of such a sensor system to about 1-2 seconds should be possible by optimizing the overall sensor size and top beam plate configurations. This should lead to a reliable, simple, spectrum-independent monitor for use in situations where very rapid response is not necessary.

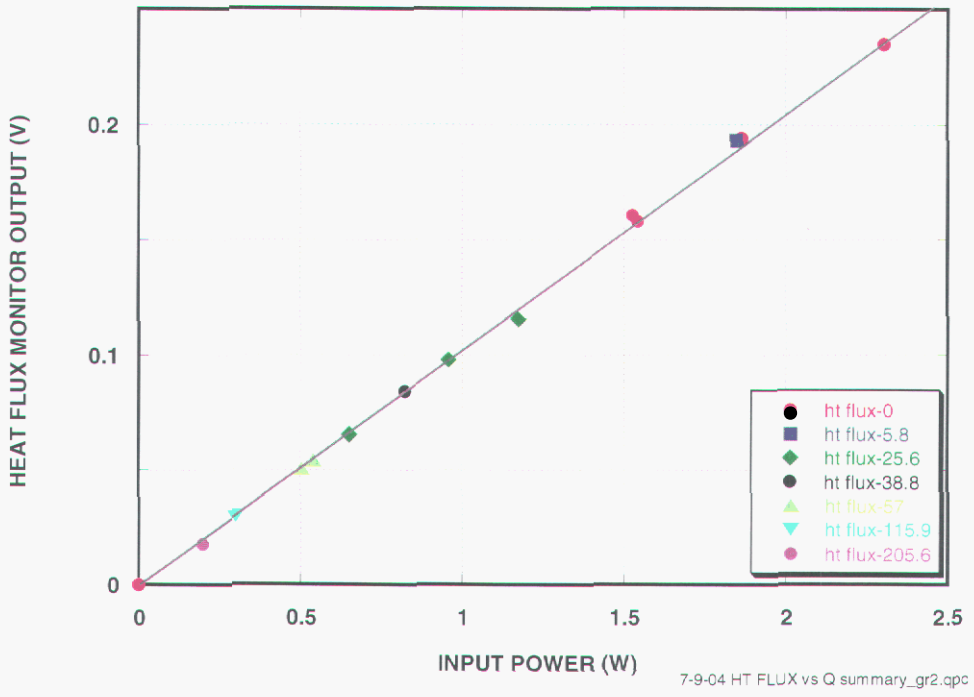

Figure 23. Output of RdF heat flux monitor versus input X-ray power

The response of the "strong-linked" calorimeter, never reached steady state in the experimental testing sequences: Because of limitations on the highest permissible temperature on the regular calorimeter block set by the epoxy used for the thermocouples, the X-ray beam was kept on for no more than about 100 seconds when filters were used. In any case, steady state temperatures were not reached in the "S-linked" calorimeters. Experimentally it was found that there was no good compromise between acceptable response times (~5 s) and easily measured temperature increases above ambient levels. Although it may be possible to develop an "S-linked" calorimeter configuration with parameters better than those in the current work, none was found in the limited experimental scope of the current program. An additional challenge with developing this type of power sensor is demonstrated by the data shown in Figure 19. The base of the S-linked calorimeter increased slowly with time, indicating that the thermal impedance between it and the water-cooled main base (see Figure 19 above) was non-zero and appreciable compared to the thermal impedance of the aluminum links. Ideally the temperature of the bottom of the S-linked calorimeter would not change under X-ray irradiation. In order to try and reduce this impedance, indium foil (~0.010" thick) was sandwiched between the S-linked calorimeter base and the main, water-cooled base. Although this strategy did reduce the upward drift in the S-linked base temperature under irradiation, it did not eliminate the increase. In light of the fact that the two other systems tested – the photodiode and heat flux sensor-based systems- showed good initial results as potential power monitors, further refinement of the S-linked calorimeter configuration was not pursued in the current studies.

5.4 Power Monitor Placement Options

Placement of a power monitor in a LIGA scanning system requires some careful consideration. If the monitor is to be used infrequently and is used only to check the input power versus nominal synchrotron operation conditions such as electron storage energy, ring current, upstream filter conditions, mirror (if any) angle setting, then the power monitor can be mounted onto a sample holder and the power can be measured statically. In this case, response time issues for the power monitor are not a concern since response times (<10 s) are much shorter than effective ring current decay constants, which are typically greater than an hour. In such applications, even a simple calorimeter similar in design to those described above could be used.

One possible application of a power monitor is its use as a process control tool during routine, X-ray exposures of samples such as occurs in the current LIGA prototyping program. If the power is to be measured while sample exposures are being performed, then its response time, the operating mode/data acquisition procedures for the monitor, and especially monitor placement all require attention. There are basically two different locations for a power monitor – either moving, on or connected to the scanning stage, or stationary, disconnected from the stage. Figure 24 below shows a principle sketch of these two regions in a LIGA exposure station.

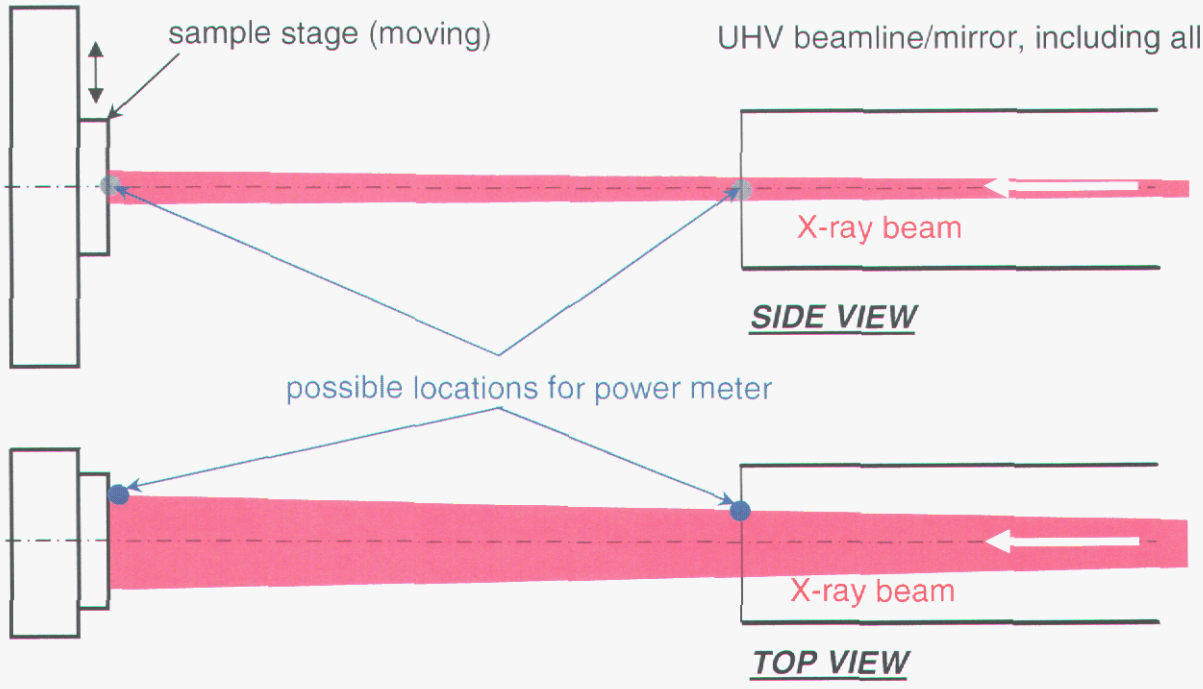

Figure 24. Possible Locations for power meters used during sample scanning located on the periphery of the X-ray fan.

In either generic location, it is required that the monitor would be located on periphery of the X-ray beam so as not to interfere with exposure of the sample on the stage. If the power meter were located on the stage and if the monitor sensing area were smaller than the scan length (~100 mm), then the main issue may be one of thermal response

time, since the monitor would only periodically intercept the X-ray beam. For instance, with a monitor detection area of ~10 mm, and a scanner speed of ~20 mm/s, the power meter would be in the beam only 10% of the time. Thus, the response time of a monitor used on the stage must be <<0.5 s, say 0.05 s. This would exclude the use of a heat flux sensor (HFS) with capture area of ~1 cm x 1 cm. Of the devices studied above, only a photodiode (PD)-based power monitoring system has the potential for a fast response time. Even when using a PD system, however, another complication arises, and that has to do with the finite size of the PD sensing area – 4 mm x 4mm in the PD tested. This area is smaller than the vertical extent of the X-ray beam (~10 mm at the ALS- see Figure 4 above). Thus, as the PD scans through the beam, the signal will vary because of the vertical, Gaussian beam profile, and a peak detection scheme with relatively high data acquisition rate (faster than 20 Hz) must be used. Such a detection scheme may be too complex not only because of the data acquisition requirements, but also because of the detailed beam profile knowledge required to interpret the data received. For the sake of simplicity and practicality, therefore, stationary power meters are probably the best choice for beam power monitors.

If the power meter were located in a stationary position, then the response time of the power meter is no longer a restriction, since the beam is constantly sampled. If the beam is constantly sampled, it is then essential to have sensor cooling; for example, when using a HFS-based power meter, a cooled substrate is required for device operation, so that the power deposited in the top absorber plate (see Figure 16) flows through the HFS and is removed. Although this cooling requirement can add to the complexity of a power monitoring system, a water-cooled, heat flux sensor-based, beam power monitor system is one which could be implemented with a high likelihood of success. As described in the results above, HFS-based systems have outputs independent of the X-ray spectrum, making them useful in the synchrotrons used in Sandia's LIGA program. In addition to being small and relatively inexpensive, HFS systems have another advantage: Since decay times for synchrotron ring currents are long compared to HFS response times, the HFS could provide essentially real time readouts of beam power and would not require sophisticated or computer-based acquisition techniques. So long as there is some peripheral region of the X-ray beam which is not used for sample exposure, as shown in the "Top View" of the sketch in Figure 24, the HFS-based power monitor is the best choice, of the systems studied above, for providing power monitoring in Sandia's X-ray LIGA exposure systems. However, as indicated in the beginning of this section, any power meter must survive and perform for long periods of time in an intense X-ray environment. Therefore, future work must be performed to determine the long term response of the HFS-based power device to extended X-ray exposure. These experiments are planned as a follow-on activity to the work described in this report.

This page intentionally left blank.

6. Summary

The results presented in Section 2 above, the initial calorimetry work on BL 3.3.1 at the ALS, show that the "new" values for the bend magnet and ring energy provide much better agreement with experiment than do the "old," default values used in LEX-D 7.56 (and LEX-D 7.54). These new values for the beam energies and magnetic fields are now the default values in LEX-D v7.61, the version of LEX-D which is current at the time of writing this report. Given accurate input data – the local bend magnet field and ring energy – the agreement between LEX-D predications and experimental results is excellent. Such agreement can only be obtained by using local field values; this underscores the necessity of having accurate values input to LEX-D for precise dose control at not only the ALS but also the APS and SSRL.

It is instructive to compare exposure times and top dose predicted by these two different versions of LEX-D. Note that the primary differences in these two versions of LEX-D are the default inputs to the code – the "old" versus "new" energy and field values. Exposure times and top doses predicted by LEX-D for a small set of sample thicknesses and filters were computed using the "old" and "new" values. These exposures were assumed to take place in either the air scanner or the vacuum scanner at the ALS beamline 3.3 at a ring energy of 1.9 GeV, mean beam current of 300 mA and scan length of 8.2 cm; a bottom dose of 3.2 kJ/cm^3 was used. The mask consisted of 25 μm of Au on a 100 μm thick Si wafer. Source to sample distances used were 18.10 m (BL 3.3.2) and 17.25 m (BL 3.3.1) The range of sample thicknesses and filters used in the calculations were chosen to represent the range of values usually used in the LIGA scanners at the ALS. Two combinations of ring parameter/databases were used: "OLD"/Biggs, which represents calculations that were used for exposure calculations done with LEX-D v7.56. "NEW"/NIST is the combination which best agrees with the experimental calorimetry work on BL 3.3.1 and is now default in LEX-D v7.61. The results for these predictions are given in Table 4 (air scanner) and Table 5 (vacuum scanner) below:

TABLE 4. Predicted exposure times and top doses in PMMA samples using "old" and "new" ring parameters (bend magnet fields and ring electron energies) and X-ray attenuation databases – BL 3.3.2, Air Scanner.

THICKNESS (μm)		"OLD"/Biggs(7.56)		"NEW"/NIST (7.61)		RATIOS (old/new)	
PMMA	FILTER(Al)	Exposure time (h)	Top Dose (kJ/cm^3)	Exposure time (h)	Top Dose (kJ/cm^3)	Exposure time	Top Dose
1500	5.6	10.64	7.45	12.40	7.53	0.858	0.989
	44.4	14.25	6.49	16.61	6.54	0.858	0.992
800	5.6	7.51	5.26	8.71	5.29	0.862	0.994
500	5.6	6.33	4.43	7.33	4.45	0.863	0.996
250	5.6	5.42	3.79	6.26	3.80	0.866	0.997

TABLE 5. Predicted exposure times and top doses in PMMA samples using "old" and "new" ring parameters (bend magnet fields and ring electron energies) and X-ray attenuation databases – BL 3.3.1, Vacuum Scanner.

THICKNESS (μm)		"OLD"/Biggs(7.56)		"NEW"/NIST(7.61)		RATIOS (old/new)	
PMMA	FILTER(Al)	Exposure time (hr)	Top Dose (kJ/cm^3)	Exposure time (hr)	Top Dose (kJ/cm^3)	Exposure time	Top Dose
1500	5.6	9.24	7.88	10.75	7.96	0.860	0.990
	38.8	12.02	6.86	14.00	6.92	0.859	0.991
	44.4	12.53	6.74	14.59	6.78	0.859	0.994
800	5.6	6.40	5.46	7.41	5.49	0.864	0.995
500	5.6	5.33	4.55	6.17	4.56	0.864	0.998
250	5.6	4.51	3.85	5.21	3.86	0.866	0.997

As the results in these tables show, there is little variation in the ratios of (old/new) values for exposure times and top doses for the combinations of PMMA/filters chosen. Top doses calculated for the two different value sets are similar, with the (old/new) ratio having at most about a 2% difference. Exposure times predicted using the default, "old" values are about 14-16% lower than with the new values. Thus, in order to achieve the proper bottom dose of 3.2 kJ/cm^3, "new" exposure times on the average will be about 15% longer than the "old" times.

In addition to helping establish a relationship between predicted and total experimental powers in these experiments at the ALS, the current work also showed the utility of making total power measurements on beamlines incorporating elements more complicated than just filters, as is the case at the ALS. The tests run at the APS clearly demonstrated the need to characterize the X-ray throughput of beamlines with mirrors, cells and other devices whose X-ray transmission characteristics can be less amenable to direct, theoretical computation of power because of device complexity and the imperfect control of beampath environmental conditions. Such situations underscore the necessity of having convenient means for measuring the total X-ray power, and led to the investigation of alternative power detection schemes, as described in Section 4. Based on the devices studied, the one most suitable for potential applications as a total power meter in all LIGA X-ray exposure systems may be a refined version of the device employing a heat flux sensor, appropriately configured so that response times are on the order of about a second or so. Although the long-term stability of such a device in an X-ray environment still must be demonstrated, better characterization X-ray power characterization and, hence, prototyping quality control in X-ray exposures should result.

In other cases, knowing more than just the total power may be important, and an indication of the total power and some measure of the X-ray spectrum may be required. In such cases, the use of filters – such as was done with the photodiode studies described in Section 5 – on different, adjacent power meters sampling different portions of the X-ray beam could offer a means of helping to determine both total power and spectral power distributions.

This page intentionally left blank.

References

1. Data regarding the bend magnet parameters were obtained through conversations with, and calculations done by, Dr. Christoph Steier of the ALS accelerator group, which is responsible for the ALS ring/magnetic lattice.

2. Koch, E-E., Handbook on Synchrotron Radiation, Vol. 1A (1983, North Holland Publishing Company, Amsterdam).

3. F. Biggs and R. Lighthill, "Analytical Approximations for X-Ray Cross Sections III," SAND87-0070, Sandia National Laboratories Report, (August 1988).

4. F. Biggs and R. Lighthill, Analytical Approximations for Total and Energy Absorption Cross Sections for Photon-Atom Scattering, SC–RR-72 0686, Sandia National Laboratories Report (December, 1972).

5. M Seltzer, J. S. Coursey, and D. S. Zucker, "XCOM Photon Cross Sections Database." http://physics.nist.gov/PhysRefData/Xcom/Text/XCOM.html; M. J. Berger, J. H. Hubbell, S.

6. Georg Aigeldinger, "Implementation of an Ultra Deep X-ray Lithography (UDXRL) System at CAMD," Ph.D. Thesis (University of Freiburg, June, 2001). Available at: http://www.freidok.uni-freiburg.de/volltexte/407/

7. Omega Engineering Thermocouple calibrator 307A.

8. ABAQUS Version 6.3, Hibbitt, Karlsson & Sorensen Inc., (2002).

This page intentionally left blank.

Appendices

Appendix A -- Cooling of the Beam Plate Under Vacuum

As indicated in the "Experimental" section above, there was cooling of the calorimeter block even when the exposure was done in "vacuum." Although the work was done in a vacuum scanner, the pressures (~0.020 Torr) still may not have been low enough to eliminate thermal conduction between the beam plate and the water-cooled base plate of the calorimeter. In order to help determine the degree of this thermal conduction, the cooling of the beam plate was measured under vacuum and under about 100 Torr of helium. The results are shown in Figure 25 below.

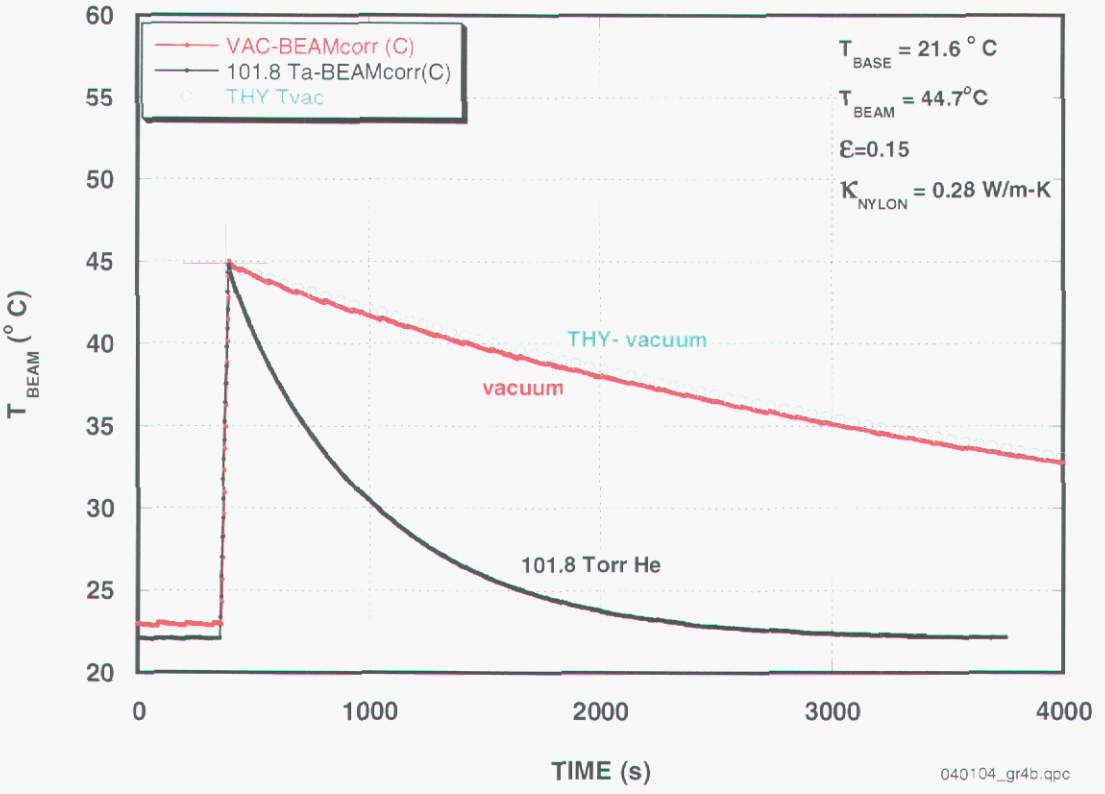

Figure 25. Cooling curves for calorimeter in vacuum and different He pressures.

In this figure, the starting times associated with data were offset so that the cooling started at essentially the same time. It is clear that cooling is substantially increased by the presence of helium gas.

The cooling under vacuum (red curve), the condition under which essentially all data in Section 1 of the report were taken, was modeled assuming discrete calorimeter elements. The predicted cooling curve is shown in blue circles. The two, primary heat loss mechanisms assumed under vacuum were conduction through the calorimeter

nylon support posts plus radiation from the calorimeter block itself. Conduction through the thermocouple leads was calculated to be five orders of magnitude less than that of the nylon posts and was therefore neglected. The value for the thermal conductivity of nylon used in the calculation was 0.28 W/m-K, well within the range of published nylon values of (0.26 - 0.30) W/m-K. The aluminum emissivity chosen was 0.15, again a reasonable value for non-anodized aluminum. Although these values are unique, the results of the simple modeling show that reasonable choices for the thermal parameters of the calorimeter can produce good agreement between predictions and the experimental data. When the calorimeter block is heated to about 45°C, the initial heat loss due to radiation is about 2.5 times greater than that due to conduction through the nylon posts to the baseplate. These results show the importance of radiative cooling of the calorimeter even when under vacuum, a factor resulting from the low thermal conductance of the nylon posts.

Modeling the cooling curves in a gaseous helium environment is not as straightforward as the vacuum case because of the necessity of accounting for all the non-planar conduction paths between the heated beam plate and the cooled base plate and chamber walls. This calculation was not pursued in detail since all the experimental work was done under vacuum.

Appendix B -- Detailed Inputs for LEX-D 7.56 for Calculations

The following inputs were used for the code inputs:

"Old Value" predictions
In "Specify synchrotron source"

[4] synchrotron source - use "ALS-1.9" or "ALS-1.5" with default values for magnetic field, ring energies
[5] beam length = 17.25 meters, the source point to vacuum scanner distance

In "Specify exposure conditions"
[2] scan length = 10.0 cm
[3] filter set

1	Be	254 μm
2	Al	(or other filter material)
3	He	0 μm
4	PMMA	(whatever is being run)
5	Kapton	(whatever is being run)

[5] mean beam current = 320 mA

When the question"* Do you want to see dose details (y/n)?" appears, <Y> is entered. The "Bottom Flux" (in W/cm^2) exiting the last filter listed in the filter sequence displayed is used as the power flux to the calorimeter. In turn, the total power to the calorimeter = 9.0 cm (beam width- see Figure 4 above)× 10.0 cm= 90 cm^2 × the "Bottom Flux" is the total power(W) to the calorimeter predicted at 320 mA ring current.
"New Value" predictions

In "Specify synchrotron source"
[4] synchrotron source - use "Custom" with the bend radius (or magnetic field), ring energy given by the "new" values in Table 1 above; use 400 mA max. ring current.

All the remaining steps are the same as in the "Old Value" predictions procedures given above.

Appendix C -- Numerical Results for Calorimetry Experiments, ALS Vacuum Scanner, Beamline 3.3.1

Spreadsheet with experimentally determined powers (expressed as W/m), LEX-D predicted values (corresponds to results shown in Figure 6). The table gives the experimental date, code numbers (internal bookkeeping), experimental results and compares the experimental results with LEX-D predictions for three cases of LEX-D:

1) LEX-D, using the original values for the bend field, ring energy and Biggs data base ("THY(Biggs)-OLD);
2) LEX-D, using the new values for the bend field, ring energy and Biggs data base ("THY(Biggs)-NEW); and
3) LEX-D, using the new values for the bend field, ring energy and NIST data base ("THY(NIST)-NEW").

All powers are in W/m, and experimental temperature rises (°C/s), calorimeter heat capacities (J/K) are listed, as are the ratios of the experimental results to the different theoretical predictions. Note that different calorimeter beamplates were used in some of the experimental runs. This fact is reflected in the differences in the heat capacities ("C", under "Experiment").

				EXPERIMENT			THY(Biggs)-OLD		THY(Biggs)- NEW		THY(NIST)- NEW	
date	sequence	Added Filter *	I.D. No.	dT/dt	C	P	P	exp/thy	P	exp/thy	P	exp/thy
				(C/s)	(J/K)	(W/m)	(W/m)		(W/m)		(W/m)	
4/14/2004	1.5GeV											
	a	none	1	0.10476	44.739	52.08	53.45	**0.974**	53.76	**0.969**	51.91	**1.003**
	b	38.8 um Al	3	0.01567	44.739	7.79	8.17	**0.953**	8.18	**0.953**	7.88	**0.988**
	c	5.8 um Al	2	0.06143	44.739	30.54	31.50	**0.969**	31.79	**0.961**	30.71	**0.994**
		values at 5.6um		0.06143	44.739	30.54	31.97	**0.955**	32.11	**0.951**		
	1.9 GeV											
	d	5.8 um Al	2	0.40615	44.739	201.90	242.50	**0.833**	215.10	**0.939**	210.74	**0.958**
		values at 5.6um		0.40615	44.739	201.90	244.40	**0.826**	216.90	**0.931**		
	e	38.8 um Al	3	0.19600	44.739	97.43	117.80	**0.827**	100.70	**0.968**	98.21	**0.992**
	f	none	1	0.57916	44.739	287.90	321.70	**0.895**	289.50	**0.994**	282.71	**1.018**
remaining data at 1.9 GeV												
4/1/2004		none-in vacuum	1	0.57377	44.739	285.22	321.70	**0.887**	289.50	**0.985**	282.71	**1.009**
		in 101.8 Torr He	1	0.57377	44.739	285.22	321.70	**0.887**	289.50	**0.985**	282.71	**1.009**
3/11/2004		98.4 um Al	5	0.09999	44.739	49.71	64.09	**0.776**	53.15	**0.935**	51.43	**0.966**
		98.4 um Al	5	0.10086	44.739	50.14	64.09	**0.782**	53.15	**0.943**	51.43	**0.975**
2/25/2004		none	1	0.56807	45.281	285.81	321.70	**0.888**	289.50	**0.987**	282.71	**1.011**
		none	1	0.57121	45.281	287.39	321.70	**0.893**	289.50	**0.993**	282.71	**1.017**
		147.6 um Al	6	0.07028	45.281	35.36	46.17	**0.766**	37.67	**0.939**	36.29	**0.974**
		147.6 um Al +500um PMMA	7	0.06019	45.281	30.28	39.53	**0.766**	32.01	**0.946**	30.68	**0.987**
		147.6 um Al +1000um PMMA	9	0.05212	45.281	26.22	34.41	**0.762**	27.69	**0.947**	26.40	**0.993**
		147.6 um Al +1500um PMMA	10	0.04579	45.281	23.04	30.35	**0.759**	24.28	**0.949**	23.02	**1.001**
		49.2 um Al	4	0.16832	45.281	84.69	102.60	**0.825**	87.12	**0.972**	84.86	**0.998**
		98.4 um Al	5	0.10140	45.281	51.01	64.09	**0.796**	53.15	**0.960**	51.43	**0.992**
2/6/2004		none	1	0.27898	90.749	281.30	321.70	**0.874**	289.50	**0.972**	282.71	**0.995**
		147.6 um Al	6	0.03594	90.749	36.24	46.17	**0.785**	37.67	**0.962**	36.29	**0.999**
		147.6 um Al +1524um PMMA	11	0.02305	90.749	23.24	30.17	**0.770**	24.13	**0.963**	22.86	**1.017**
		147.6 um Al +3048um PMMA	12	0.01697	90.749	17.12	21.74	**0.787**	17.13	**0.999**	15.99	**1.070**
1/29/2004		147.6 um Al 2-1s	6	0.02672	118.926	35.31	46.17	**0.765**	37.67	**0.937**	36.29	**0.973**
		147.6 um Al 2-1s	6	0.02727	118.926	36.04	46.17	**0.781**	37.67	**0.957**	36.29	**0.993**
		147.6 um Al +516um KAPTON	8	0.02239	118.926	29.59	38.55	**0.768**	31.23	**0.948**	29.85	**0.991**
		none	1	0.22475	118.926	296.98	321.70	**0.923**	289.50	**1.026**	282.71	**1.050**

This page intentionally left blank.

Initial Distribution:

3 Honeywell Federal Manufacturing & Technologies
Attn: Larry Zawicki, MS-MD40
Madhuri Widmer, MS-MD40, Dept. EE8
B. L. Dearth, MS-FH40
P. O. Box 419159
Kansas City MO 64141

1 Lawrence Berkeley National Laboratory
Attn: C. A. Steier, MS 80R0114
1 Cyclotron Road
Berkeley, CA 94720

1	MS9004	J. M. Hruby, 8100
1	MS9161	S. K. Griffiths, 8350
1	MS9401	S. W. Allendorf, 8753
1	MS9401	G. Aigeldinger, 8753
1	MS9401	D. R. Boehme, 8753
1	MS9401	L. L. Hunter, 8753
5	MS9401	M. E. Malinowski, 8753
1	MS9401	S. Mrowka, 8753
1	MS9401	D. M. Skala, 8753
1	MS9401	C. Solf, 8753
1	MS9402	C. D. Moen, 8752
5	MS9402	A. Ting, 8752
1	MS9402	J. E. M. Goldsmith, 8772
1	MS9404	G. D. Kubiak, 8750; Attn:
	MS9409	P. Spence, 8754
	MS9953	J. A. Lamph, 8755
1	MS9405	K. L. Wilson, 8700 (Actg.); Attn:
	MS9161	B. Even, 8760
3	MS9018	Central Technical Files, 8945-1
1	MS0899	Technical Library, 9616
1	MS9021	Classification Office, 8511 for Technical Library, MS0899, 9616 DOE/OSTI via URL

This page intentionally left blank.